Recent Material Developments in Fast Oxide Ion Conductors

J. C. Boivin and G. Mairesse

Laboratoire de Cristallochimie et Physicochimie du Solide (URA CNRS 452), Ecole Nationale Supérieure de Chimie de Lille, Université des Sciences et Technologies de Lille, B.P. 108, 59652 Villeneuve d'Ascq Cedex, France

Received April 2, 1998. Revised Manuscript Received July 21, 1998

Over the past decade, many efforts have been made to develop new materials exhibiting high oxide ion mobility at low temperature. In addition to the improvements of existing materials, new classes of conductors in which the structure have been shown to play an important role has been proposed. These materials are reviewed according to their structure type. Their performances and limitations are presented and discussed.

Contents

Introduction

Oxide ion conductors are an exciting class of materials and are involved in an increasing number of application domains. Oxide ion conduction is a specific property of some solids that was discovered more than a century ago by Nernst in zirconia derivatives. Because of the lack of high performance materials, applications of oxide electrolytes were confined, for a long time, to specific domains that do not need high current densities; for instance, oxygen sensors. The reason for this confinement is that oxide ion is a big (radius (r) ∼ 1.40 Å) double-charged ion that strongly interacts with the cation network. High mobility of such a species implies very specific structural features. To reduce the operating temperature and/or to allow high current densities, many research works have been performed to improve the known materials (mainly, zirconia-based electrolytes) and to find new phases or families of materials more able to satisfy the increasing variety of needs. Because of both of these aspects, great strides forward have been made and oxide ion conductors now have realistic possibilities for development in the near future in fuel cells, dense membranes for oxygen separation, and catalysis. Several reviews papers have already been devoted to oxide conductors,[1−7] usually focusing mainly on a specific class of materials. In the present review, we take a tentative overall structure-oriented approach to the most recent results obtained on this important topic.

Fluorite-Type Oxide Electrolytes

From a historical point of view, this class of materials has been the most widely investigated, mainly because of the extensive research works conducted on stabilized zirconia for applications in solid oxide fuel cell (SOFC). Pure ZrO_2 exhibits three different crystallographic polymorphs, monoclinic, tetragonal, and cubic, respectively, depending on the temperature. The distorted tetragonal and cubic fluorite polymorphs are built on the basis of a Zr^{4+} cation fcc packing with oxide ions located in the tetrahedral sites of the structure (Figure 1). To get oxide conduction properties, part of Zr^{4+} must be substituted by another cation with a lower valence state (mainly Ca^{2+}, Sc^{3+}, Y^{3+}, or a rare-earth cation). This doping leads first to stabilization of the cubic or the tetragonal form, depending on the synthesis temperature and the dopant concentration. Second, to achieve the electrical neutrality, vacancies are simultaneously created in the anion network. The ionic conductivity of stabilized zirconia at a given temperature depends on the nature and the concentration of the aliovalent cation. The radius of this cation plays a major role. The conductivity (σ) increases as the radius becomes close to that of Zr^{4+} ($r_{VIII} = 0.84$ Å). The best value is reached for Sc^{3+} ($r_{VIII} = 0.87$ Å) with a σ value equal to 10^{-1} S cm^{-1} at 800 °C for $(ZrO_2)_{0.9}(Sc_2O_3)_{0.1}$. For the sake of comparison, the σ value for $(ZrO_2)_{0.9}(Y_2O_3)_{0.10}$ at the same temperature is close to 3×10^{-2} S cm^{-1} ($r^{Y3+}_{VIII} = 1.02$ Å). As previously mentioned, substituting Zr^{4+} with an aliovalent cation creates oxide vacancies leading for a 3+ cation to a defect solid solution which can be formulated $Zr_{1-x}M_xO_{2-x/2}\square_{x/2}$. As a consequence, the extrinsic conductivity first quickly increases and then, despite the linear increasing of the number of vacancies with x, always decreases. Typically, σ exhibits a sharp maximum for $0.08 \leq x \leq 0.12$.

10.1021/cm980236q CCC: $15.00
Published on Web 10/02/1998

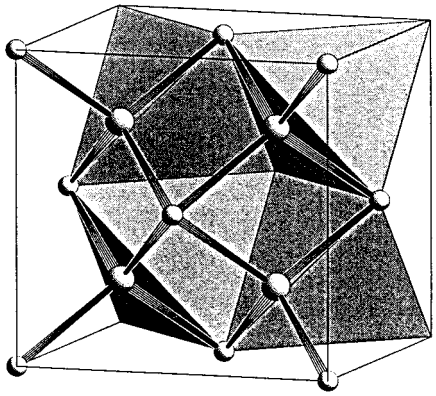

Figure 1. Schematic view of the fluorite structure.

This result can be explained by defect interactions between doping cations and vacancies that can no longer contribute to the conduction process.

If a high conductivity is an essential parameter for a solid electrolyte to be suitable for applications, many other conditions must be fulfilled to provide a reliable operating device. Most of the experimental fuel cells are now designed using yttria-stabilized zirconia with $x = 0.08$. The main reason for that design is the high chemical stability of this phase, both toward anode (H_2 or CO) reduction and cathode (air or pure O_2) oxidation. However, the limited oxide conductivity of stabilized zirconia electrolytes and the need to reach current densities of several hundred mA cm^{-2} to satisfy economical requirements implies that the SOFC must operate at high temperature (800−1000 °C). Such high temperatures lead to many technological problems, such as mechanical instability, materials aging, and undesirable chemical reaction between cell components (electrolyte, electrodes, interconnecting material...).

To lower the operating temperature, extensive research has been conducted to look for new fluorite materials with conductivity values larger than those of zirconia-based electrolytes. Some simple structural considerations led to the conclusion that the choice is necessarily limited. It is clear from the structure that to leave a tetrahedral crystallographic site, the oxide ion must cross a bottleneck limited by three cations located at the vertexes of one of the triangular faces of its coordination tetrahedron. The simplest way to make this crossing easier is to occupy the cation sites with polarizable cations. As the polarizability of an ion increases with its radius, big cations must be preferred. However, to maintain the stability of the fluorite structure, the ratio between the cation and the anion radii must remain close to 0.70. On the basis of an oxide ion radius of 1.38 Å, the optimum cation size is close to 1 Å. Such a large radius is typically of the order of magnitude of that of 4f elements. Because of the lanthanide contraction with the atomic number, only elements located at the beginning of the lanthanide series can ideally fit the size requirement.

Ceria solid solutions have been widely investigated. As expected, their conductivity is higher than that of zirconia-based phases. For instance, the conductivity of a cerium gadolinium mixed oxide is about five times that of the corresponding yttrium zirconium oxide. Among ceria-based electrolytes, samarium-doped ceria exhibits the highest ionic conductivity.[8] However, under reducing conditions, Ce^{4+} is easily reduced to Ce^{3+}, leading to an electronic contribution to conductivity. In addition to the loss of efficiency, Badwal et al.[9] have noticed a large increase in the grain boundary impedance associated with the formation of Ce^{3+} near the grain boundary regions. After reoxidation, the distortion of the lattice impedance arc is characteristic of microcracks development. This result would seriously limit the use of cerium-based electrolytes in SOFC. However, in a very recent work, Huang et al.[186] have observed little impedance at the grain boundaries of reduced ceria.

Different authors have proposed coating cerium-based electrolytes with a thin layer of yttria stabilized zirconia.[10,11] This process leads to suppression of the electronic contribution without significant increase of the overall resistance of the cell, but a reaction occurs between doped ceria and stabilized zirconia that can preclude a long-term use of this system.[12] Materials containing CeO_2 could, however, be used in mixed ionic electronic membranes (MIEC) for oxygen gas separation or syn-gas preparation. Nigara et al.[13] have reported an oxygen flux of 13×10^{-6} μmol cm^{-2} s^{-1} at 870 °C using a $Zr_{0.45}Ce_{0.09}Ca_{0.36}O_{1.44}$ membrane.

Looking for highly polarizable cations, special attention has been focused on p-type external orbital metal oxides. These elements exhibit a high polarizabilty due to their electronic structure that is characterized by the presence of a nonbonding electronic pair. The most interesting are those that have the largest ionic radius. Among them, Bi^{3+} quickly appeared as a very attractive cation. Its $6s^2$ pair is known to be highly stereochemically active. Numerous structural studies led to the conclusion that this pair usually occupies a mean volume of the same order of magnitude as that of an oxide ion. This specificity generates very loose and deformable structures that are particularly suitable for anion migration.

High conductivity of bismuth oxide and bismuth mixed oxides has been first reported by Takahashi et al.[14] Bi_2O_3 is a polymorphic oxide and many contradictory investigations have been performed before the description made by Harwig and Gerards,[15,16] which is considered as the most correct one. Only two varieties are stable. The low temperature α form is monoclinic. It converts at 729 °C into the face-centered cubic δ form, which is stable up to the melting point at 824 °C. On cooling, large thermal hysteresis occurs and the metastable tetragonal β or body-centered cubic γ form can be obtained depending on the cooling conditions. The α-monoclinic and γ-bcc forms are semiconductors, whereas the β-tetragonal and δ-fcc forms are oxide ion conductors. The highest conductivity occurs with the δ form. The structure of the δ form is highly disordered (the thermal effect associated to the $\alpha \Rightarrow \delta$ transition is nearly three times larger than the heat of melting). This form derives from the fluorite structure but, because of the stoichiometry ($BiO_{1.5}\square_{0.5}$), the anion network contains 25% intrinsic vacancies without any need for doping. According to Battle et al.,[17] the cations are arranged as a cubic close packing and oxide ions occupy two sites of the $Fm3m$ space group: 43% of the regular $^1/_4$ $^1/_4$ $^1/_4$ sites are randomly occupied and the remaining 1.28 oxide anions per unit cell relax in the ⟨111⟩

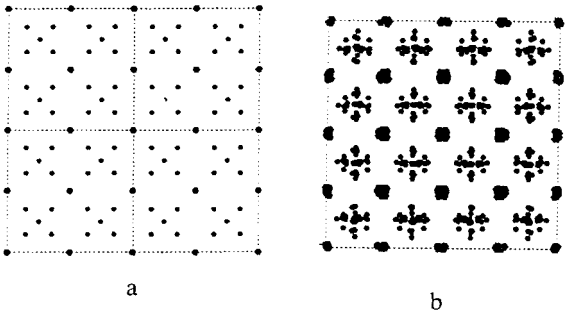

Figure 2. Comparison of oxide ion disorder in δ-Bi_2O_3 form (a) BATTLE[17] and (b) DEPERO. Reprinted with permission from ref 18. Copyright 1996 Academic Press.

direction and are displaced from their ideal position to a *xxx* ($x = 0.354$) site. In a recent paper, Depero et al.[18] propose a somewhat different distribution of the oxide ions that is also characterized by a dramatic disorder. Figure 2 compares the projection of the two structures along the [100] axis.

From these results, it is quite clear that the high temperature δ-Bi_2O_3 form exhibits several unique features: high polarizability of the cation network, highly disordered anion network, presence of 25% intrinsic vacancies, and large ability of bismuth cations to dynamically accommodate asymmetric surroundings. These characteristics are together responsible for the very high conductivity of δ-Bi_2O_3, which exhibits a σ value 2 orders of magnitude larger than that of stabilized zirconia: $\sigma_{730\ °C} = 1$ S cm^{-1}.[19] A further and determining advantage of Bi_2O_3 is its favorable catalytic effect on the oxygen dissociation reaction, which is always the first and often limiting step in every electrochemical process involving oxygen transfer. Several works on bismuth derivatives have emphasized the high activity of bismuth-based surface compared with that of noble metals. This effect was clearly evidenced using a bismuth lead oxide electrolyte, which was shown to easily support high current densities using a special cell design in which the electronic surface conductivity was provided by means of a thin gold grid co-sintered with the electrolyte.[20,21] In a general study of the oxygen transfer process, Boukamp et al.[22] have also evidenced that the exchange current densities obtained for porous sputtered platinum or gold electrodes on a bismuth-based electrolyte are almost identical; that is, that "electrode material" nature has little influence on the oxygen transfer rate, in contrast with observations performed under the same conditions on zirconia-based electrolytes.

However, the δ-Bi_2O_3 form is only stable at temperature higher than 730 °C up to its melting point (830 °C). This limited range of stability and the mechanical stress associated with the volume change during the phase transitions make pure Bi_2O_3 unsuitable for practical applications. As a consequence, cation substitution, which is not needed because of the presence of intrinsic vacancies in oxygen network, has been performed to stabilize the highly conductive δ form below the phase transition temperature.

The choice of cations that can be used is very large because, in contrast with ZrO_2, isovalent (= 3) and even higher valence state cations (>3) can be used. Numerous oxides from divalent up to hexavalent elements have been studied.

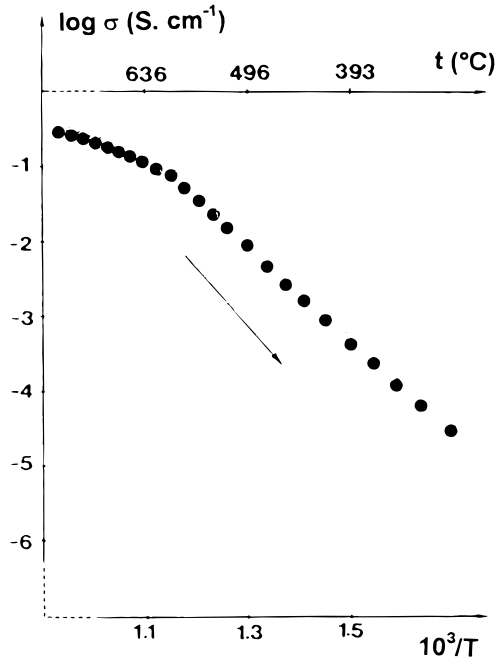

Figure 3. Arrhenius plot of $(Bi_2O_3)_{0.75}(Y_2O_3)_{0.25}$ conductivity.

For M^{2+} cations (M = Ca, Sr, Ba, Pb),[23−29] a large domain of fcc solid solution exists at high temperature but is difficult to preserve at room temperature: the larger the cation size, the narrower the range of stabilization that completely vanishes for Ba and Pb.

Isovalent cations have been the most extensively investigated (M = Y, Ln).[40−49] Figure 3 shows a typical example of conductivity curve for M = Y. As usual, this curve exhibits two domains with different activation energies that have been related to a short-range ordering at low temperature. Considering the results obtained with yttria-stabilized zirconia, many authors have investigated the Bi_2O_3−Y_2O_3 fluorite solid solution.[30−41] In the equilibrium domain of the fcc phase, the conductivity progressively decreases with increasing dopant concentration. This trend is general in the doped δ phase, which can be related, at least partly, to the lower polarizability of the dopant cation compared with that of Bi^{3+}. In the stabilized domain at lower temperature, a maximum in the conductivity occurs for $(Bi_2O_3)_{0.75}(Y_2O_3)_{0.25}$. Most of the elements belonging to the lanthanum series have also been investigated. The best conductivity is obtained with erbium oxide for the composition $(Bi_2O_3)_{0.75}(Er_2O_3)_{0.25}$.[42] The δ-type phases have also been reported with M^{4+} (M = Te),[35] M^{5+} cations (M = V, Nb, Ta),[31,48] and W^{6+}.[49]

Many controversies arose about the effective stability of the fcc phase at low temperature. For Verkerk et al.,[42] the stabilization results from a contraction of the δ structure and is therefore better achieved with small ionic radius cations. The lowest Ln_2O_3 concentration needed to stabilize the δ structure is 0.15 for Er_2O_3. Watanabe[50−52] studied a large number of δ-Bi_2O_3-stabilized phases, particularly for M = Te, La, Nd, Sm, Eu, Gd, Dy, Ho, Er, Tm, Yb, Lu, Pr, Tb, Nb, Ta, and W, and concluded that the δ phase cannot be readily stabilized by an oxide addition. All the reported "stabilized" δ phases are quenched phases or fcc-based tetragonal phases.

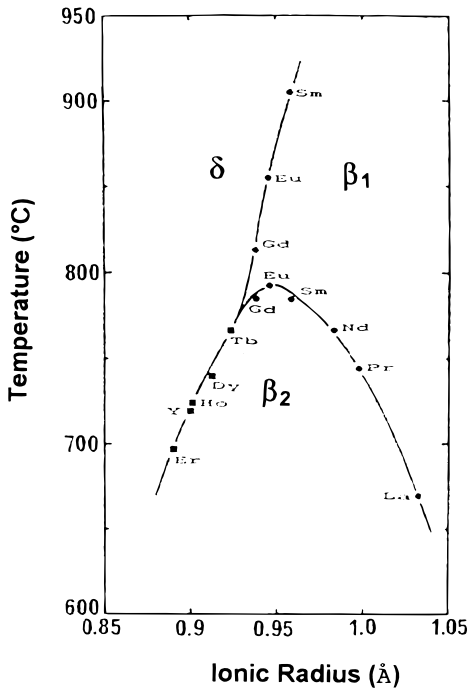

Figure 4. Polymorphism dependence on ionic radius for $Bi_{0.775}Ln_{0.225}O_{1.5}$. Reprinted with permission from ref 53. Copyright 1993 Elsevier.

When annealing at low temperature (typically <700 °C), the quenched δ phases progressively convert into a stable phase. The time necessary for the transformation to occur varies from some hours to several weeks. The most common transformation leads to the formation of one of both β_1 or β_2 polymorphs of a layered rhombohedral phase that will be described later.

Watanabe et al.[53] have also examined the polymorphism dependence on the ionic radius in $Bi_{0.775}Ln_{0.225}O_{1.5}$ for Ln = Y, La−Er. Figure 4 summarizes the results. The maximum of stability for the δ phase, which corresponds to the lowest temperature for entering the equilibrium domain, is encountered for erbium. Then the temperature increases gradually as the ionic radius increases. Up to terbium, a direct-phase transition occurs from the low temperature β_2 rhombohedral phase to the δ phase. For larger ionic radii, the transition occurs in two steps according to the $\beta_2 \Rightarrow \beta_1 \Rightarrow \delta$ sequence.

Ionic conductivity measurements performed during long-time annealing led to the conclusion that a progressive decay of the conductivity occurs, even in the absence of any trace of cubic ⇒ rhombohedral transformation. That is the case, for instance, for samples with composition $(Bi_2O_3)_{0.80}(Er_2O_3)_{0.20}$ whose conductivity decreases with time upon annealing at temperatures <600 °C. The fastest decay rate occurs at 500 °C.[54,55] Investigations performed by various techniques [X-ray diffraction (XRD), differential scanning calorimetry (DSC), and transmission electron microscopy (TEM)] led to the conclusion that this aging is related to an ordering of oxygen vacancies that is characterized on electron diffraction patterns by the appearance of satellite spots along the ⟨111⟩ direction.[56] For Fung et al.[57] the time constant of the conductivity decay is too large to be associated with the ordering of anion vacancies whose time constant is several orders of magnitude smaller. They examined in detail the effect of aliovalent dopants on the phase transformation kinetics and ordering in Bi_2O_3−RE_2O_3 solid solutions (RE = Yb, Er, Y, Dy)[58] and confirm that the stated low-temperature transformation of yttria- or rare-earth-based cubic δ phase solid solution to a rhombohedral phase is a general feature. The temperature range and the kinetics of this transformation depend on the nature and the concentration of the dopant. At low temperature (typically at temperatures <600 °C for $(Bi_2O_3)_{0.80}(Er_2O_3)_{0.20}$ samples), a superstructure appears in the cubic solution that is responsible for the conductivity decay. This ordered superstructure is also metastable and is in relation with the stable rhombohedral phase. Both phenomena, cubic ⇒ rhombohedral and disordered cubic ⇒ ordered cubic, are governed by cation diffusion, the different kinetics of the two processes being related to the differences in characteristic diffusion distances. The cation ordering hypothesis is supported by the X-ray structure factor calculations and by the observation that the only reflections present are those corresponding to a bcc lattice with a cell parameter about twice the δ phase one. The decrease of the conductivity is associated with differences between Bi−O and RE−O bond strength.

In a recent study, performed by neutron diffraction on a $(Bi_2O_3)_{0.80}(Er_2O_3)_{0.20}$ powdered sample, Jiang et al.[59] compared the structural differences between an unaged sample and a sample annealed for 330 h at 500 °C. The unaged sample exhibits structural parameters in good agreement with previous results obtained by Battle[17] in Y^{3+}- and Er^{3+}-doped Bi_2O_3. They found two cations distributed over a 0.05, 0, 0 site. The oxide ions are distributed in 8c (0.25, 0.25, 0.25), 32f (0.309(1), 0.309(1), 0.309(1)), and 48i (0.5, 0.313(8), 0.313(8)) crystallographic sites with occupation factors equal to 1.00(9), 1.64(13), and 0.36(7), respectively. After aging, the main difference concerns the 8c site whose occupation factor drops down to 0.01(7), whereas the 32f one increases up to 2.61. This result is accompanied by a small lowering of the x coordinate ($x = 0.037(2)$) of the cation site and a reduction of 2% of the cell parameter ($a_{\text{unaged}} = 5.500(2)$ Å; $a_{\text{aged}} = 5.492(2)$ Å). The main change during aging is the displacement along the ⟨111⟩ direction of 33% of the oxide ions that were initially located in the ideal tetrahedral site of the fluorite-type structure. The remaining question is whether the oxide ions and vacancies are ordered. Jiang et al.[56] proposed a superstructure arrangement with an oxygen vacancy ordering in the ⟨111⟩ direction. For this superstructure to be consistent with TEM observations (mainly the occurrence of a body-centered lattice), oriented microdomains with three ordering directions must exist. Such a condition has been confirmed using high-resolution TEM. However, the authors underline that if anion ordering alone can explain the electron diffraction patterns, this ordering does not preclude the additional possibility of a simultaneous cation ordering.

In a recent paper, Watanabe,[60] performing very-long-time annealing (1500 h at 800 °C), stabilized a bcc $Bi_{1-x}Ln_xO_{1.5}$ phase (Ln = Sm−Dy) with a cell parameter about twice that of the δ phase. The structure was solved by Drache et al.[61] using XRD and the Rietveld method in the space group $I2_13$. The parameters are summarized in Table 1. Bismuth ions fully occupy two

Table 1. Atomic Coordinates for the bcc $Bi_{0.65}Gd_{0.35}O_{1.5}$ Phase

element	Wyckoff position	occupation factor	*x*	*y*	*z*
Bi(1)	8a	1	0.2702(2)	0.2702(2)	0.2702(2)
Bi(2)	12b	1	0.0163(4)	0.0	0.25
Bi(3)	12b	0.066	0.4979(6)	0.0	0.25
Gd	12b	0.934	0.4979(6)	0.0	0.25
O(1)	24c	1	0.373(3)	0.079(5)	0.388(4)
O(2)	24c	1	0.127(4)	0.349(3)	0.139(4)

crystallographic sites whereas the third cation site is statistically occupied by the remaining Bi ions and all the Gd ions. The ordered cation sublattice corresponds to positions slightly shifted from their theoretical ones in the fluorite subcell. Each cation surrounding is constituted by an ordered distribution of six anions and two vacancies. The similarity between the characteristics of this phase and the conclusions about cation and anion distribution in a bcc arrangement deduced from TEM experiments is strong. However, the synthesis conditions are quite different. Watanabe's phase[60] is obtained after a prolonged annealing process at 800 °C (i.e., at a temperature located ~200 °C above the range in which the δ phase progressively converts into a rhombohedral phase). Conversely, the TEM results indicated that the bcc phase was obtained after annealing samples at only 500 °C. Some additional experiments are needed to clarify this point. However, Drache's structural study[61] clearly demonstrates the possibility, at least at 800 °C, for cation and anion ordering to occur simultaneously.

The possible existence of a correlation between (cation and/or anion) ordering and superstructure formation or phase transformation seems in agreement with the reported increase of stability of the low-temperature δ form when two or more cations are used to substitute for Bi^{3+}. According to Meng et al.,[62] who studied different $Bi_2O_3-(Y_2O_3, MO_x)$ double-dopant-systems (M = Nb, Gd, Sm, Pr), the minimum dopant content for stabilizing the δ form is lower than with single-dopant systems. This cooperative stabilization effect is attributed to the corresponding increase of entropy in the multi-doped materials. A similar trend has been evidenced in the $Bi_2O_3-CaO-PbO$ system.[63] Although the δ form cannot be stabilized in both Bi_2O_3-CaO and Bi_2O_3-PbO binary systems, δ can be preserved over a large range of composition using a double Ca^{2+}, Pb^{2+} substitution for Bi^{3+}. The same enhancement of δ stability was also observed when using a seven-rare-earth-dopant system.[64]

The favorable effect of the dopant polarizability on the ionic conductivity has been reported by Omari et al.[65] in the system $Bi_2O_3-Y_2O_3-PbO$. For the same dopant concentration, the conductivity increases as the Pb^{2+}/Y^{3+} also increases (Figure 5).

Among double-dopant systems, high conductivity has been recently reported within the Bi−Ln−V−O (Ln = Y, Sm−Dy, Er, Yb) systems.[66] The best performances were evidenced with Ln = Tb whose samples exhibit the highest conductivity and the lowest activation energy. For instance, the conductivity of $Bi_{0.85}Tb_{0.105}V_{0.045}O_{1.545}$ is 10^{-3} S cm^{-1} at 300 °C compared with 0.5×10^{-4} S cm^{-1} for $Bi_{0.8}Er_{0.2}O_{1.5}$ at the same temperature. The reason for introducing V^{5+} as a dopant was to increase the number of mobile oxide ions per unit cell and to take advantage of the catalytic effect of V^{5+} ions on oxygen dissociation toward the cathode reaction.

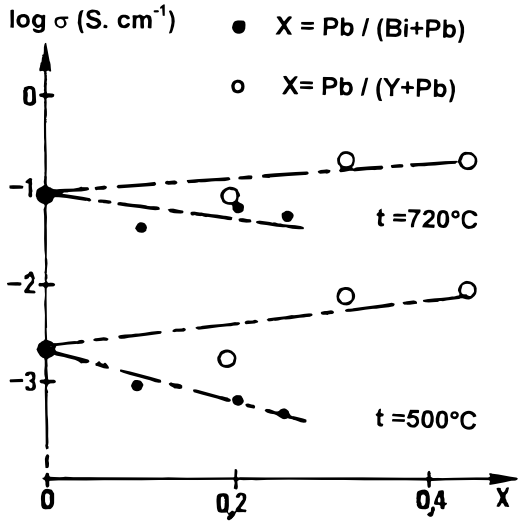

Figure 5. Composition dependence of σ for (●) $Bi_{0.65(1-x)}Y_{0.35}Pb_{0.65x}O_\delta$ and (○) $Bi_{0.65}Y_{0.35(1-x)}Pb_{0.35x}O_\delta$. Reprinted with permission from ref 65. Copyright 1990 Elsevier.

The comparison of the addition effect of CaO and ZrO_2 upon δ stability has been examined by Fung et al.[58] In this study, 2% CaO and 5% ZrO_2 were respectively added to samples corresponding to $(Bi_2O_3)_{0.80}-(RE_2O_3)_{0.20}$ samples (RE = Er, Yb, Y, Dy). The authors observe a similar effect for the different RE samples. For instance, in the case of bismuth−erbium oxide, the time constant associated with the $\delta \Rightarrow$ rhombohedral transformation for the undoped and CaO-doped samples annealed at 600 °C were nearly 330 and 55 h, respectively. On the contrary, no noticeable transformation occurs in the ZrO_2-doped sample. A similar trend is observed for the conductivity decay that was evidenced, even in the absence of any trace of $\delta \Rightarrow$ rhombohedral transformation (at least within the first period of the experiments) for samples annealed at temperatures ≤500 °C. However, the kinetics of conductivity decay are faster than those for cubic ⇒ rhombohedral phase transformation. Figure 6 shows that the corresponding time constant for undoped and 5% ZrO_2-doped sample is a linear function of the stabilizer ionic radius, which is in good agreement with a correlation between this evolution and cation diffusion facility. A similar study has been performed by Huang et al.[67] on CeO_2 added to the $(Bi_2O_3)_{0.75}-(Y_2O_3)_{0.25}$ electrolyte. They confirm the severe aging problem of this electrolyte if annealed at 600−650 °C. Addition of 5 mol % CeO_2 (the solubility limit being 9%) leads to the optimum oxide ion conductivity and suppresses the cubic ⇒ rhombohedral phase transformation. The presence of tetravalent cations that tend to repel oxygen vacancies from their nearest-neighbor coordination was shown to block the cooperative atomic diffusion that is necessary for the phase transformation to occur. During this study, attention was also drawn to the importance of the associated cathode material, and the oxygen-deficient perovskite $La_{0.6}Sr_{0.4}Co_{0.2}Fe_{0.8}O_{3-\delta}$ was shown to provide a very efficient oxygen electrode material.

Using a combined approach by Rietveld and microstructural analysis, Sooryanarayana et al.[68] recently proposed a mechanism of stabilization for a δ sample

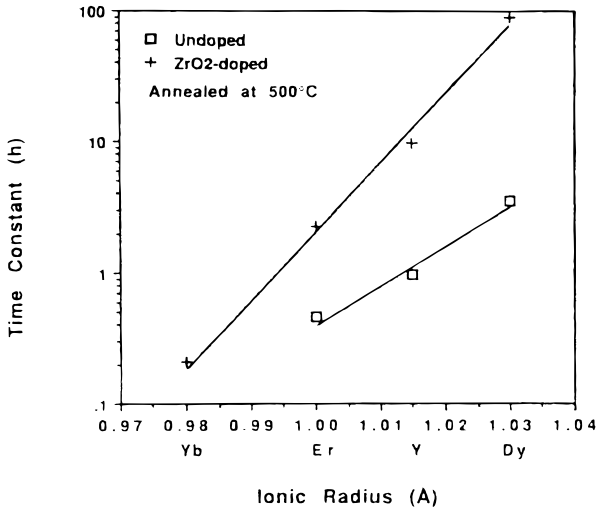

Figure 6. Aging time constant comparison between undoped and 5% ZrO_2-doped samples versus the stabilizer ionic radius. Reprinted with permission from ref 58. Copyright 1993 American Ceramic Society.

with $Bi_{1.6}Ho_{0.4}O_3$ composition. According to the Willis or Harwig models, Bi^{3+} and Ho^{3+} are distributed over the 4a Wickoff position of the $Fm3m$ space group whereas the six oxide ions are located in the 32f site (*xxx* with $x = 0.3615(80)$). From microstructure analysis, using an adjustable model to minimize the difference between calculated and experimental normalized intensity values, they get an estimated enthalpy that allows evaluation of the degree of stabilization of a doped material. The calculated value for the holmium-doped phase ($\alpha^* = 0.03$) is lower than that calculated for the pure δ ($\alpha^* = 0.07$) or α Bi_2O_3 ($\alpha^* = 0.05$) form. Such an approach is proposed to evaluate the degree of stabilization of a low-temperature δ phase. However, taking into account the difficulty to precisely solve the structure of the highly disordered δ-type phases even when using neutron diffraction experiments, the results obtained from powder XRD should be interpreted very cautiously, especially concerning the oxide ions distribution whose X-ray diffusion factor is very low when compared with that of Bi^{3+} ions.

Rhombohedral-Type Oxide Electrolytes

As previously mentioned, most of the bismuth oxide-based systems show the existence, in their Bi_2O_3-rich part, of a rhombohedral phase first reported by Sillen.[69] This phase exhibits high oxygen mobility at moderate temperature.[25,70,71] Conductivity values are usually close to 1 S cm^{-1} at temperatures around 700 °C. The stability domain of the rhombohedral phase as a function of the dopant concentration strongly varies with the characteristics of the doping cation. For instance, with alkaline-earth cations, the maximum stability range occurs with Sr^{2+} and the minimum with Ba^{2+}.[28,29,72]

Conductivity curves usually exhibit a dramatic reversible jump at a temperature that is strongly dependent on the nature of the dopant.[25,68,70] This jump is related to an order−disorder phase transition that results in a sudden increase of the *c* parameter and is accompanied by a large enthalpy change. The structure of the two polymorphs, β_2 and β_1 for the low- and high-temperature forms, respectively, was solved by Boivin et al.[73] and Conflant et al.[72] The structure of β_2 is represented in Figure 7. It is a layered structure built up from covalent blocks stacked along the c direction of the hexagonal cell. Each block contains three cation layers. The two external layers only accommodate bismuth cations, whereas the central layer contains the doping ions and the remaining bismuth cations. Two anion sites were detected. The first one (O_1) is located near the center of the blocks, and oxide ions on this site are strongly bonded to cations. The second one (O_2) is located at the periphery of the blocks. The remaining highly delocalized anions were not detected by XRD but geometrical considerations led to the conclusion that they were necessarily located between the blocks and considered as mainly responsible for the conduction properties. This hypothesis was supported by single-crystal conductivity measurements (Figure 8), which emphasize a strong anisotropic character.[74] Their location was later confirmed and precisely determined by neutron diffraction.[75−77] It is worth noticing that the oxide ion conduction layer is bordered on both sides by a bismuth layer. Examination of the corresponding

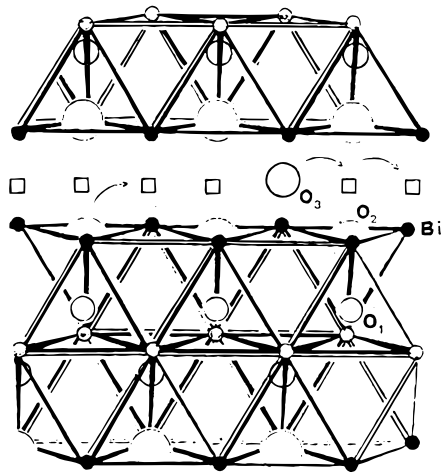

Figure 7. β_2-Polymorph structure of rhombohedral phases. Reprinted with permission from ref 72. Copyright 1983 Elsevier.

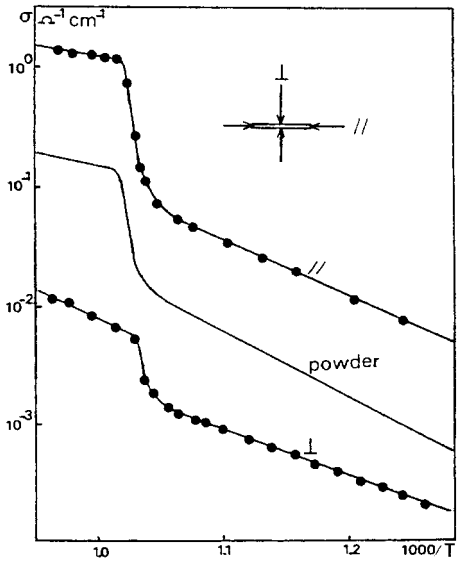

Figure 8. Single-crystal conductivity measurement on a $Bi_{0.851}Sr_{0.149}O_{1.425}$ rhombohedral phase. Reprinted with permission from ref 74. Copyright 1981 Elsevier.

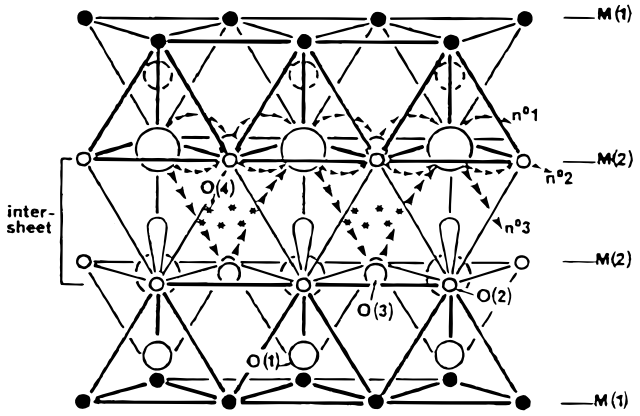

Figure 9. Structure of the β_1-rhombohedral polymorph. Reprinted with permission from ref 75. Copyright 1994 Academic Press.

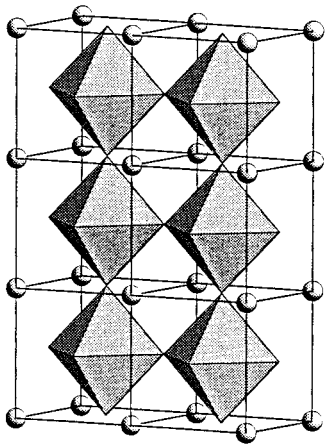

Figure 10. Polyhedron stacking in perovskite-type structure.

bismuth ion coordination polyhedron clearly indicates that their $6s^2$ nonbonding electronic pair is oriented toward this layer and must play an important role in the conduction process. This is a common feature of the bismuth-based ionic conductor-layered structures.

High-temperature X-ray and neutron crystal structure determination showed, at the $\beta_2 \rightleftharpoons \beta_1$ transition, an increase of both the delocalization and the number of anions in the conduction layer at the expense of those located near the periphery of the blocks (O_2 site). This evolution versus the temperature is presented in Figure 9.[75] The β_1 and β_2 structures have a close relationship with the δ structure. The $\beta \Leftrightarrow \delta$ transition consists of a shift from an (ABC)−(BCA)−(CAB) sequence (rhombohedral symmetry) to an (ABC)−(ABC)−(ABC) sequence (cubic symmetry). This shift only involves a relative glide of the blocks within the conduction layers. This glide is particularly easy because the chemical bonds there are very weak because of the high mobility of the oxide ions in these layers.

The rhombohedral phases are thermodynamically stable phases. So, many works have been focused on them for developing applications. One of their weaknesses could be the occurrence in most cases of a $\beta_2 \Leftrightarrow \beta_1$ transition. However, this transition is quite soft; that is, most of the structural features are maintained through the transition. Moreover, both low- and high-temperature phases are pure ionic conductors. To evaluate the possible use of rhombohedral phase in SOFCs, Baek and Virkar[78] examined the stability of alkaline-earth derivatives in a reducing atmosphere. The best results were obtained for $(Bi_2O_3)_{1-x}-(SrO)_x$ samples with $x = 0.43$. The $p(O_2)$ reduction (8×10^{-14} atm at 630 °C) is four times lower than for pure Bi_2O_3. However, this value still remains too high for application in SOFC. These authors claimed that the stability may be strongly enhanced by coating the bismuth-based electrolyte with a thin layer of zirconia on the side exposed to the fuel.[79]

The layered rhombohedral alkaline-earth oxide conductors have also been used recently for iodine intercalation.[80,81] In agreement with the structural and electrical features, iodine is intercalated in the conduction layer. As a consequence, the *a* parameter is little affected by the intercalation process. On the contrary, an expansion for the *c* parameter of 9 Å has been observed (i.e., 3 Å per layer). The Raman spectra show evidence of I^{3-} species and possibly of I^{5-} species. The behavior of this phase is very similar to that observed for bismuth cuprate high T_c superconductors and could offer opportunities for new developments.

Perovskite-Type Oxide Electrolytes

Materials that adopt the very stable perovskite-type structure are involved in many domains where high performance electrical properties are needed. These domains include electronic conductors, ferroelectric materials, and high T_c superconductors. The reason perovskite-type oxide electrolytes are desirable in these situations is the great geometrical and chemical flexibility of the perovskite structure. The ideal structure is presented in Figure 10. This structure corresponds to the basic formula ABO_3 were A can be a single-charged, 2^+, or 3^+ cation, and B, depending on the A oxidation state, is a 5^+, 4^+, or 3^+ cation, respectively. Depending on the relative size of A and B ions, the ideal cubic symmetry of the unit cell may progressively lower according to the importance of the deviation of the $(R_A + R_O)/(R_B + R_O)$ ratio from the ideal $\sqrt{2}$ value.

Substitution of A or/and B cations by aliovalent dopants is, like in fluorite materials, an easy way to introduce vacancies in the anion network that may lead to significant oxygen mobility. It must however be emphasized that a too large number of vacancies can induce structural deformations. A strong lowering of the lattice symmetry will be clearly incompatible with high oxygen mobility because of the noncrystallographic equivalence of the different vacancy and oxygen sites. The oxygen vacancies may also become ordered as, for instance, in the brownmillerite structure.

From an historical point of view, perovskite phases have been first considered as possible electrode materials for SOFCs, and numerous studies have been devoted to various doped lanthanum manganites and cobaltites exhibiting high electronic conductivity and specific electrochemical activity toward oxygen dissociation.

The first report of the existence of oxide conductivity in a perovskite material was made by Takahashi et al.[82] on a calcium-doped lanthanum aluminate, but the discovery of really attractive oxygen conduction properties is rather recent. Some of these research works were dictated by the predictive approach of Cook and Sammels[83] who define three optimized criteria for a high

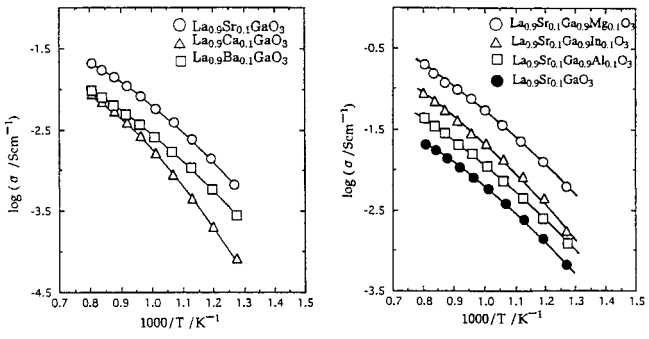

Figure 11. Effect of various cations substitution for La and Ga sites in $LaGaO_3$ at $p(O_2) = 10^{-5}$ atm. Reprinted from ref 86. Copyright 1994 American Chemical Society.

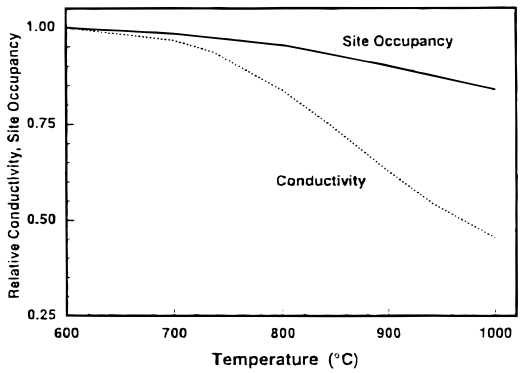

Figure 12. Relative changes in site occupancy and conductivity of $La_{0.6}Sr_{0.4}Co_{0.2}Fe_{0.5}O_3$ as a function of the temperature. Reprinted with permission from refs 89, 90. Copyright 1995 Elsevier.

oxide ion conductivity in perovskite materials: a low mean value of metal−oxygen bonding energy, an open structure (high free volume), and a critical cation bottleneck for O^{2-} migration as large as possible. These criteria mean that both the A and B cation radius and valence state are determining factors.

Two types of materials have been investigated aiming at different industrial applications: pure and mixed ionic electronic conductors. One of the first attempts to find a competitive perovskite ionic conductor was made by Goodenough et al.[84] The best performances are obtained with doped $LaGaO_3$ perovskite. Feng et al.[85] proposed a new doped perovskite both on the A and B sites, $La_{0.9}Sr_{0.1}Ga_{0.8}Mg_{0.2}O_{2.85}$, whose conductivity at 750 °C is close to 0.1 S cm^{-1}. These results are in agreement with those published at nearly the same time by Ishihara et al.[86] who studied the effect of various dopants at the La and Ga sites on the conductivity (Figure 11). On the La and Ga sites, the best results among the alkaline-earth cations are obtained for Sr^{2+} and Mg^{2+}, respectively. The use of electropositive dopant cations allows one to dispose of a stable material under low oxygen partial pressure with conductivity values higher than those obtained for zirconia- and ceria-based fluorite electrolytes. For instance, the conductivity was shown to be insensitive to $p(O_2)$ down to 10^{-20} atm for samples $La_{0.9}Sr_{0.1}Ga_{1-x}Mg_xO_3$ ($0 \le x \le 0.15$) at 1123 K.

The same authors extended their study to the family $(La_{0.9}Ln_{0.1})_{0.8}Sr_{0.2}Ga_{0.8}Mg_{0.2}O_{3-\delta}$, with Ln = Y, Nd, Sm, Gd, or Yb.[87] The conductivity decreases in the order Nd > Sm > Gd > Yb > Y. This variation is an illustration of the effect of the crystal lattice symmetry on the oxygen mobility: the conductivity decreases linearly with the departure (tolerance factor) from the ideal ion radii ratio for a cubic perovskite structure. Among the different samples investigated, the most promising material has the composition $(La_{0.9}Nd_{0.1})_{0.8}Sr_{0.2}Ga_{0.8}Mg_{0.2}O_{2.8}$. The presence of a small amount of Nd in the La site leads to suppression of any hole conduction in the high oxygen partial pressure range. This material exhibits a pure ionic conduction (0.5 S cm^{-1} at 1223 K) from 1 to 10^{-21} atm between 1000 and 1300 K.

As previously pointed out, many defect perovskite materials offer the opportunity, under appropriate oxygen partial pressure, to combine ionic and electronic conductivity. For this reason, perovskite materials are particularly investigated as mixed conductors for developing pressure-driven dense membranes. Such membranes are able to separate oxygen without the need of an external power source and are particularly attractive for syn-gas (CO/H_2) production directly from natural gas such as methane. For such an application, the material must be able to provide high oxygen flux. That means, a high total conductivity with an optimized ionic−electronic balance over a large range of oxygen partial pressure.

Terakoa et al.[88] investigated double-doped (A and B sites) perovskites and evidenced that the $La_{1-x}Sr_xCo_{1-y}Fe_yO_{3-\delta}$ family exhibits attractive oxygen permeation properties associated with a good efficiency toward oxygen reduction, particularly when the number of different transition metals in the B site increases. Because of these results, special attention has been focused on this family, and the oxygen fluxes dependence on x and y values has been extensively investigated. The precise electronic and ionic properties strongly depend on these values because they determine, as a function of the temperature, both the mean valence of mixed A and B sites and the departure from O_2 stoichiometry (i.e., the number of vacancies and the correlated anionic mobility).

Tai et al.[89,90] reported that in the $La_{1-x}Sr_xCo_{0.2}Fe_{0.8}O_3$ system, the samples belong to the perovskite type up to $x \le 0.4$. The electronic contribution is p type and due to hopping of small polarons, the charge carriers are created by the Sr^{2+} acceptor dopant and by Co^{3+} disproportionation into Co^{2+} and Co^{4+}. The Sr content is compensated by a double mechanism: the formation of Fe^{4+} ions and the creation of oxygen vacancies, their relative proportion being temperature dependent. As a consequence, the total conductivity decreases from 600 °C (Figure 12). This decrease was attributed both to the decrease of the carrier concentration and to their lower mobility due to a scattering mechanism by oxygen vacancies whose number increases with the temperature.

In the $(La,Sr)(Fe,Co)O_x$ system, Balachadran et al.[91] have reported a new mixed conducting phase $SrFeCo_{0.5}O_x$ in which the ionic and electronic conductivity contribution are both high and nearly equal at 800 °C in air. The oxide ion transference number is close to 0.4, and the activation energy for ionic conduction is only 0.37 eV. This phase, with B/A cation site occupation equal to 1.5, is neither a purely cubic perovskite nor a

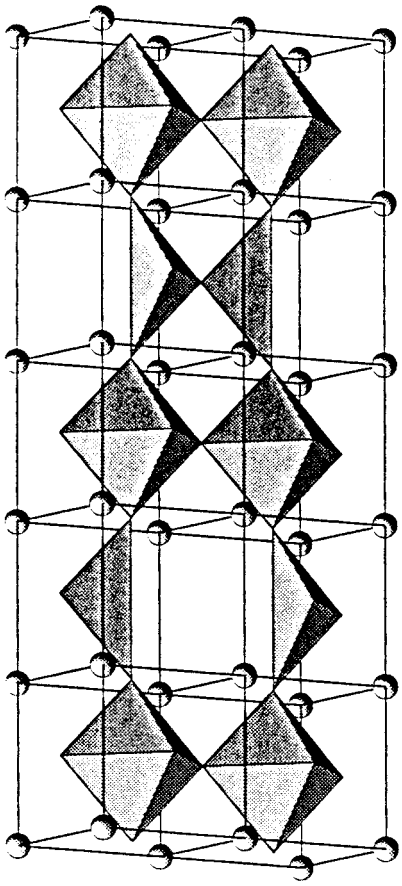

Figure 13. Schematic brownmillerite structure.

brownmillerite-type material in which the corresponding ratio is unity. The mixed conductivity arises from a Frenkel disorder in the oxygen sublattice.[92] This material was shown to deliver oxygen fluxes varying from 6 to 10 mL cm^{-2} min^{-1} in the range 850−950 °C.

Brownmillerite Oxide Electrolytes

The general formulas of a brownmillerite oxide is $A_2BB'O_5$ (from the original mineral Ca_2FeAlO_5) but in several attractive oxide conductors, B and B′ are identical. The brownmillerite structure is closely related to the perovskite one; they only differ by the oxygen vacancy distribution. Phase transitions often occur in brownmillerite materials versus the temperature and are accompanied by an increase of the disorder, so the frontier between disordered brownmillerites and true oxygen-deficient perovskites is not always clearly delimited.

In oxygen-deficient perovskites, the vacancies are statistically distributed over all the oxygen sites leading to the characteristic 3-dimensional network of corner-sharing octahedra. The brownmillerite structure contains 16.66% intrinsic oxygen vacancies that are ideally ordered along the [110] direction, but some more complex distributions can occur. Starting from the perovskite octahedra-linking model, a row of equatorial oxygen is missing every two rows in alternate (001) BO_6 layers. (Figure 13). This pattern results in a new stacking sequence with alternate BO_6 distorted octahedra perovskite (O) and BO_4 corner-sharing tetrahedra layers (T): ...OTOTOT.... The corresponding orthorhombic cell is related to the cubic perovskite one by the relations: $a_{orth} \cong a_{cub}\sqrt{2}$, $b_{orth} \cong 4c_{cub}$, $c_{orth} \cong a_{cub}\sqrt{2}$.

The first report of significant oxygen mobility in a brownmillerite structure phase was made by Goodenough for $Ba_2In_2O_5$.[93] The conductivity at 800 °C is close to 10^{-3} S cm^{-1} (for $p(O_2) = 10^{-6}$ atm) and jumps to 10^{-1} S cm^{-1}after an order−disorder transition in the oxygen-vacancy network. The exact nature of this transition has been studied using various high-temperature techniques by Adler et al.[94] These authors arrived at the conclusion that the transformation occurs in two steps. At the transition temperature, the tetrahedral layer converts into a deficient octohedral perovskite layer O_D, and the structure remains orthorhombic with a ...$OO_DOO_DOO_D$... sequence. At higher temperature, the vacancy disorder extends to all the layers, leading to a pure oxygen-deficient ...$O_DO_DO_DO_DO_DO_D$... cubic perovskite sequence.

The aliovalent doping strategy was used in these materials to stabilize one of the two high-temperature forms. Goodenough[93] substituted cerium for indium. For the composition $Ba_2In_{1.75}Ce_{0.25}O_{5.125}$, the conductivity jump is no longer observed. However, a break occurs at a temperature close to 850 °C. In the low-temperature region, the conductivity is ∼1 order of magnitude higher than the conductivity of $Ba_2In_2O_5$, typically 10^{-2} S cm^{-1} at 700 °C, but somewhat lower at temperatures above the $Ba_2In_2O_5$ order−disorder transition. The activation energy at high temperature is nearly the same in both the doped and undoped materials. The lower conductivity in the high-temperature range is probably due to the decrease of the total number of vacancies. The increase of activation energy below the break may be attributed to an additional trapping energy due to the presence of the aliovalent dopant cations.

Several other $ABO_{5\pm\delta}$ brownmillerite-type phases have been proposed by substituting for barium and/or indium. The best performances have been reported for the double-substituted $Ba_2(GdIn_{1-x}Ga_x)O_5$ solid solution, which exhibits a conductivity value of 5×10^{-3} S cm^{-1} at 600 °C.

Several brownmillerites and related phases were shown to be highly sensitive to moisture, leading to unexpected high O^{2-} conductivities at low temperature. This result is particularly true when substituting Zr^{4+} for In^{3+}. Goodenough[95] paid particular attention to this problem and analyzed the reasons for the behavior in $BaZr_{1-x}In_xO_{3-0.5x}$. The conclusion was that the large Ba^{2+} ion stabilizes 12-fold oxygen coordination and Zr^{4+} stabilizes 6−8 oxygen near neighbors. Therefore, water diffuses into the oxygen-deficient network to provide greater coordination to the cations, leading to proton conduction. These "fast oxygen conductors" are, in fact, attractive proton conductors at moderate temperature (≅300−700 °C). This problem (when looking for oxide-ion conductors) can, however, be overcome by substituting La for Ba rather than Zr for In. Goodenough[95] reports that $(Ba_{1.2}La_{0.8})InO_{5.4}$ has an oxide ion conductivity (10^{-2} S cm^{-1} at 700 °C) very close to that of yttria-stabilized zirconia but it also degrades with time at 800 °C.

During a study of $Ba_2In_2O_5$ stability, Zhang et al.[187] emphasized the reducibility of In^{3+} ions leading to

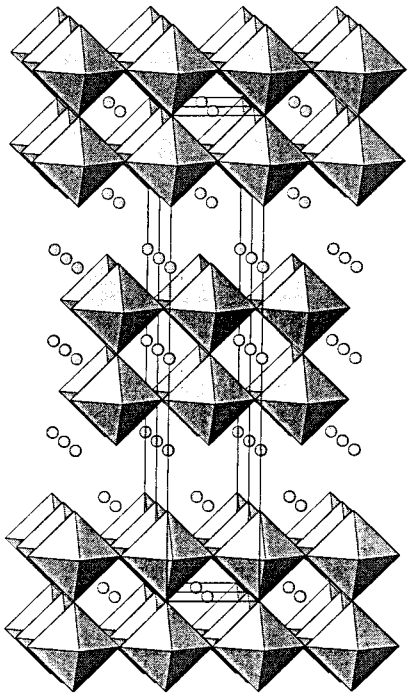

Figure 14. Schematic Ruddlesden−Popper phase structure.

n-type conduction for even modestly reducing atmospheres. $Ba_2In_2O_5$ was also shown to degrade in CO_2 atmosphere with formation of $BaCO_3$ and loss of In_2O_3. These authors suggested replacing In^{3+} with an element with a more stable 3^+ oxidation state, like Y, Er, or Ga. When investigating the Ba−In−O for stabilizing new fast-layered-structure oxide conductors around 400 °C, Goodenough et al.[96] revealed another family with the general formula $Ba_3In_2MO_8$ (M = Zr, Hf, Ce). This idea was supported by the publication of a paper from Abraham et al.[97] which emphasized the exceptional oxide ion conductivity of an Aurivillius-type layered structure. Searching for new materials in which perovskite blocks alternate with other layers along the c-axis to give an intergrowth structure, Goodenough and co-workers[98] considered $Ba_3In_2MO_8$ as the second term ($n = 2$) of an intergrowth of a ...$(O)_nT$... series in which the $n = 1$ term corresponds to the brownmillerite and the $n = \infty$ corresponds to the perovskite structure. However, later careful examination of these materials led these authors[98] to conclude that the actual structure was cubic with disordered oxygen vacancies. As for the $Ba_2In_2O_5$-type phases, proton conduction must take place at moderate temperature. As a general law, it seems, from these results, that the T layer increases the sensibility to moisture by making insertion of H_2O molecules easier.

Ruddlesden−Popper-Type Oxide Ion Electrolytes

The search for new highly conductive intergrowth structures in which perovskite layer(s) alternate(s) with one or several different structure type layers led Navas et al.[5] to get interested in Ruddlesden−Popper phases. The general formula of these phases can be written $A_{n+1}B_nO_{3n+1}$. The structure consists of n ABO_3 perovskite layers sandwiched between two AO rock-salt layers (Figure 14). $Sr_3Ti_2O_7$, for instance, corresponds to the $n = 2$ term of the series. The first evaluation of the conductivity of these phases was conducted by Turillas et al.[99] on $Sr_3Ti_{1.9}M_{0.1}O_{7-x}$ (M = Al^{3+}, Mg^{2+}). Navas et al.[5] extended their study by carrying out substitutions in the B site of the perovskite layers of $Sr_3(M_{2-x},M'_x)O_{7-x/2}$ with M = Ti^{4+}, Zr^{4+} and M′ = Al^{3+}, Ga^{3+}, In^{3+}. They reported the conductivity variation for $0 \le x \le 0.20$. The best conductivity at 950 °C is equal to 1.6×10^{-3} S cm^{-1}, which is nearly identical for M = Ti^{4+} and M′ = Ga^{3+} ($x = 0.25$) or In^{3+} ($x = 0.10$). Activation energies lie in the range 0.8−0.9 eV during cooling cycles. However, a high p-type contribution to the conductivity was observed at high $p(O_2)$ ($>10^{-5}$ atm). In the range 10^{-5}−10^{-15} atm, the conductivity is mainly ionic (independent of $p(O_2)$) but remains very low: 10^{-5} S cm^{-1} at 700 °C. The authors provide a possible explanation involving the 2-dimensionality for the low ionic conductivity when compared with other oxygen-deficient perovskite materials. The reason could be a bit more complex because of the behavior of some brownmillerite phases. The limited number of investigated phases and the lack of precise structural data do not allow definitive conclusions to be drawn about the ability of these types of material to provide useful oxide electrolytes

Pyrochlore Oxide Electrolytes

The pyrochlore structure has received careful attention for a long time because of the high-temperature stability and the various potential domains of applications of materials that adopt this structure. Pyrochlore materials can be used as solid electrolytes, oxygen electrodes, catalysts, and so on. The general formula $A_2B_2O_6O'_{1-\delta}$ illustrates the well-known ability of the structure to accommodate oxygen nonstoichiometry. The pyrochlore structure belongs to the $Fd3m$ space group. The bigger A cation is located in the 16d site (0.5, 0.5, 0.5), and the smaller B cation is in the 16c site (0, 0, 0). Six oxygen atoms are in a 48f site (x, 0.125, 0.125), whereas the remaining oxygen atoms partly or fully occupy the 8b site (0.375, 0.375, 0.375). The structure can be described as an ordered, oxygen-deficient fluorite structure. It contains 25% oxygen vacancies for the stoichiometry $A_2B_2O_7$ (i.e., one vacancy per fluorite cubic unit cell). Because of the ordered vacancy distribution, the cubic unit cell parameter of the pyrochlore is twice the fluorite one. Eight fluorite cubes are needed to fully describe the pyrochlore arrangement. These cubes can be divided in two groups. In type I cubes, the oxygen vacancy is located in the 3/4, 3/4, 3/4 tetrahedral site of the fluorite cell, and in type II cubes, the vacancy is located in the 1/4, 1/4, 1/4 tetrahedral site. In the pyrochlore structure, types I and II are arranged in such a way that a type I cube shares faces only with type II cubes. This representation (Figure 15) offers the advantage of easily determining the correlation with the fluorite structure. Another approach consists of describing the structure as built up from corner-sharing B_2O_6 octahedra. This network provides large 3-dimensional hexagonal tunnels along which are running (−A−O−A′−) chains. These chains easily accommodate oxygen and cation nonstoichiometry, leading when both anion and cation are missing to the WO_3 pyrochlore structure.

The most extensive research on pyrochlore oxide electrolytes has been conducted by Tuller's group from

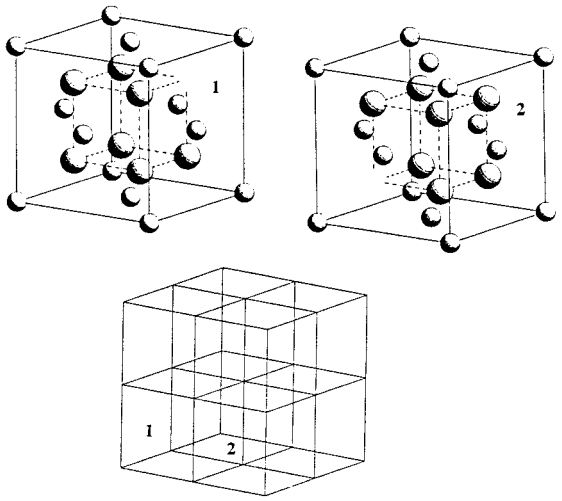

Figure 15. Schematic pyrochlore arrangement. Reprinted with permission from ref 183. Copyright 1994 Elsevier.

Cambridge, MA.[100,101] They focused their investigations on $Gd_2Ti_2O_7$- and $Gd_2Zr_2O_7$-based conductors in particular. The $Gd_2(Ti_{1-x}Zr_x)_2O_7$ solid solution is of a great interest because the $x = 0$ member is an ionic insulator whereas the $x = 1$ end member is a very good oxide ion conductor. As a consequence, the x value enables one to control the σ_i/σ_e ratio over several orders of magnitude. Doping of the "A" site with Ca^{2+} and the "B" site with Al^{3+} in $Gd_2Ti_2O_7$ has been performed by Tuller et al.[101] For calcium-doped samples, the ionic conductivity at 1000 °C quickly increased from 10^{-4} S cm^{-1} for pure $Gd_2Ti_2O_7$ up to 5×10^{-2} S cm^{-1} for samples doped with $x = 10\%$ mol of Ca^{2+}. For higher Ca^{2+} doping rates, the conductivity remains nearly constant up to $x = 15\%$. This value exceeds the conductivity of $Gd_2Zr_2O_7$ and is within a factor of 2 of that for yttria-stabilized zirconia. As usually observed, the activation energy decreases as the ionic conductivity increases; it varies from 0.94 eV for $Gd_2Ti_2O_7$ down to 0.63 eV for the 10% doped sample. A similar trend was observed for the low Ti^{4+}/Al^{3+} doping values ($x \leq 0.10$). At higher dopant concentration, the conductivity quickly decreases. Conductivity measurements as a function of $p(O_2)$ indicate a significant dependence of the ionic and electronic relative contributions on the calcium dopant concentration. All samples exhibit n-type conductivity at low $p(O_2)$, ionic conductivity at intermediate $p(O_2)$, and p-type conductivity at high $p(O_2)$. The most striking feature is the rapid extension of the ionic domain as the Ca^{2+} ratio increases. For instance, at 800 °C, the electrolytic domain of a 0.25% Ca^{2+}-doped sample extends from 10^{-4} to 10^{-12} atm, this domain ranges from 10^{-1} to 10^{-20} atm for 5% Ca^{2+}-doped samples. These studies showed that doped pyrochlore may exhibit conductivity values with the same order of magnitude as stabilized zirconia. The possibility of adjusting the electronic and ionic contributions by doping shows that optimized pyrochlores may be considered for the conception of dense MIEC membranes. As pointed out by Tuller,[101] enhanced electrode performances may be expected from MIEC in which both σ_i and σ_e are high. So, special attention has been drawn to materials in which instead of increasing σ_i at the expense of σ_e or vice versa, it was possible to boost both contributions. This effect could be achieved using multivalent acceptor elements as "B" site dopants. A satisfactory tendency has been observed with Mn-doped $Gd_2Ti_2O_7$ samples. Attractive results have also been published using Ru or Mo dopants.[102]

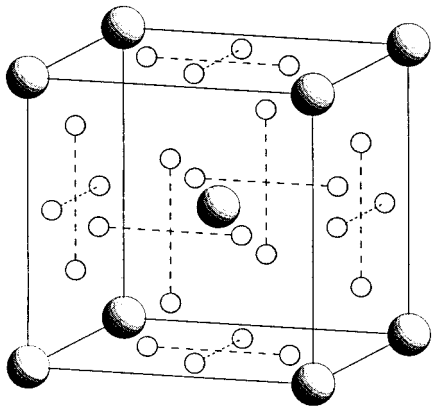

Figure 16. Anti-α-AgI-type bismuth−lead oxide structure (adjacent oxygen tetrahedral sites cannot be occupied at the same time).

Anti-α-AgI Oxide Electrolytes

The α form of silver iodide is a well-known efficient Ag^+ conductor. The conductive form is reached at 145 °C after a phase transition from the β low-temperature wurtzite-type structure to a bcc-type structure. This transition is associated with a large thermal effect (of the same order of magnitude as the heat of melting). This large thermal effect is characteristic of a large increase of the entropy of the material, something like the melting of a subnetwork, which here is the Ag^+ network that looks like a liquid. On Fourier synthesis calculated from XRD intensities, Ag^+ ions appear delocalized over a large number of sites (the tetrahedral 12d sites and the 24h intermediate sites). The presence of the highly polarizable I^- ions also contributes to the large σ values.

Honnart et al.[103] described a very similar situation in the bismuth−lead oxide system. They evidenced a large range of solid solution named β that exhibits, at 600 °C, conductivity values of the same order of magnitude as those reported for α AgI at 200 °C; that is, ~1 S cm^{-1}. The activation energy is also particularly low; that is, <0.50 eV. Transference number measurements evidenced a pure anionic conductivity. As for AgI, the phase converts on cooling into a low-temperature form: the exact nature of this form depends on the composition and the cooling conditions. Powder neutron diffraction structure investigations led to a model in which the location of cations and anions was reversed compared with α AgI (Figure 16). It is worthwhile to emphasize that the highly polarizable isoelectronic and randomly distributed Bi^{3+} and Pb^{2+} play the same role as the I^- anions in AgI. The bismuth−lead phase has been used to separate oxygen gas up to current densities of ~500 mA cm^{-2} [20,21] using mixed electrodes constituted by co-pressed gold grids at the surface of the electrolyte. Because of the strong tendency of the material to crystallize, ZrO_2 was added to the electrolyte to act as a mechanical barrier between grains to prevent them from crystal growth. This addition resulted in a net increase of the mechanical resistance of the membrane without any significant loss of the conductivity.

The highly conductive β phase was also evidenced in the Bi_2O_3−CdO, Bi_2O_3−CdO−PbO,[104] Bi_2O_3−Sb_2O_3−

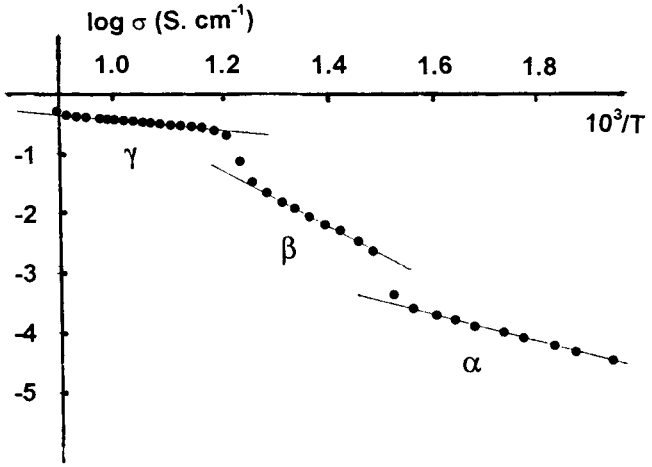

Figure 17. $Bi_4V_2O_{11}$ conductivity as a function of the temperature. Reprinted with permission from ref 107. Copyright 1988 Elsevier.

PbO, and $Bi_2O_3-Ln_2O_3-PbO$ (Ln = Gd, Dy, Tm)[105] systems. The mechanical properties of the sintered material are improved by Sb substitution. The conductivity slightly increases in the order Sb < Tm < Gd < Dy. Experiments have been conducted by Fee et al.[106] on copper- or nickel-added β samples to increase their mixed conductivity and evaluate their oxygen permeability. At 610 °C, oxygen permeated through a pellet at a rate of 10^{-6} mol min^{-1} cm^{-2}.

The anti-α-AgI oxide-type structure provides a class of materials with exceptional anionic conductivity values. No other material has ever been reported that exhibits a pure oxide ion conductivity value as high as 1 S cm^{-1} at only 600 °C. However, the highly disordered liquidlike 3-dimensional oxygen network, whose formation is associated with a strong endothermic effect (large entropy increase), necessarily appears very near the melting temperature of the sample, which precludes the use of such materials for industrial applications. However, such a structural feature offers an interesting model. One can expect that a similar liquidlike model in a layered structure would not suffer the same limitation for the temperature range of stability.

$(Bi_2O_2)(A_{n-1}B_nO_x)$ Aurivillius-Type Oxide Electrolytes

n = 1 Aurivillius-Type Electrolytes. The first evidence of high oxide ion conductivity in an alternate $(Bi_2O_2)^{2+}$ layer/perovskite layer structure was published in 1988 by Abraham et al.[107] These authors evidenced a new phase, $Bi_4V_2O_{11}$,[107] which was simultaneously reported as a new ferroelectric material in several Soviet publications.[108−112] The nonlinear properties have led to numerous publications that are out of the scope of this review.[113−121] In 1988, Abraham et al.[107] showed that $Bi_4V_2O_{11}$ exhibits two main reversible phase transitions: $\alpha \Leftrightarrow \beta$ at 450 °C and $\beta \Leftrightarrow \gamma$ at 570 °C. They emphasized the existence of a very high oxide ion conductivity in the γ-domain: 0.1−1 S cm^{-1} (Figure 17). The structure of the different forms early appeared as very complicated. The high temperature γ form crystallizes in the tetragonal *I*4/*mmm* space group with the *a* parameter close to that of the perovskite $a_p \sim 3.9$ Å. From a structural point of view, $Bi_4V_2O_{11}$ can be written $(Bi_2O_2)^{2+}(VO_{3.5}\square_{0.5})^{2-}$ and considered as the first member ($n = 1$) of the Aurivillius family, like Bi_2WO_6 or Bi_2MoO_6. The average V−O polyhedron appears as a squashed octahedron, and the different oxygen-deficient octahedra are connected by sharing corners, leading to a ReO_3 layer. The idealized γ structure, in which the oxygen vacancies have been ignored, is represented in Figure 18. On cooling, ordering of oxide ions and vacancies occurs in the perovskite layer leading for β to an orthorhombic cell with $a_\beta = 2a_p\sqrt{2}$, $b_\beta = a_p\sqrt{2}$, $c_\beta = c_p$, and for α to a monoclinic cell with $a_\alpha = 6a_p\sqrt{2}$, $b_\alpha = a_p\sqrt{2}$, $c_\alpha = c_p$, $\beta = 90.24°$. The monoclinic distortion disappears as soon as a small amount of impurities or dopant is introduced into this phase, leading to an orthorhombic symmetry.

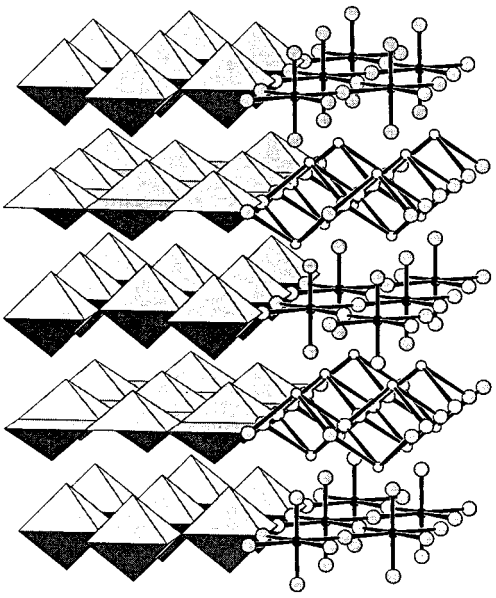

Figure 18. Idealized γ-$Bi_4V_2O_{11}$ structure.

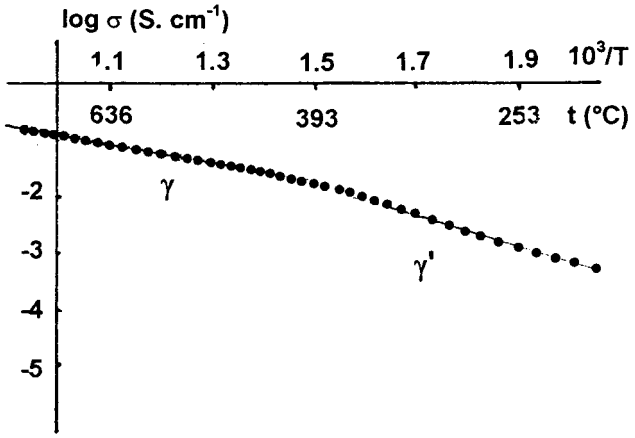

Figure 19. Arrhenius plot for BICUVOX. Reprinted with permission from ref 122. Copyright 1990 Elsevier.

Because of the very attractive conduction properties of the γ form, attempts to stabilize this phase were undertaken using a doping strategy. These attempts led to a paper from the Lille group in France[122] in which the first member of a new family of very fast oxide ion conductors named BIMEVOX was described. The BICUVOX.10 phase (BICUVOX for bismuth copper vanadium oxide) can be formulated $Bi_2V_{1-x}Cu_xO_{5.5-3x/2}$ with $x = 0.10$. The conductivity Arrhenius plot (Figure 19) shows that the phase transitions that characterized $Bi_4V_2O_{11}$ are no longer present. The plot shows the existence of

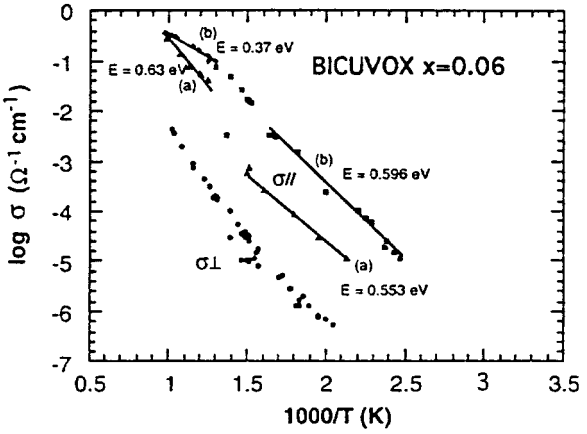

Figure 20. Anisotropic character of the conductivity in BICUVOX. Reprinted with permission from ref 130. Copyright 1994 Elsevier.

two linear γ/γ' regions with slightly different activation energies. This behavior was confirmed by different authors.[123−128] As expected, because of the layered structure, single-crystal conductivity measurements exhibit a strong anisotropic character that was observed both for $Bi_4V_2O_{11}$[129] and different BIMEVOX like BICUVOX,[128,130] BICOVOX,[131] or BINIVOX samples[130] (Figure 20).

Numerous dopants are able to substitute for vanadium and, depending on the nature of this dopant and its concentration, yield solid solutions with α-, β-, and γ/γ'-type $Bi_4V_2O_{11}$ structures. These structures correspond to a different degree of ordering and incommensurability. $Bi_4V_2O_{11}$ itself is the upper limit of a narrow solid solution domain that extends toward the Bi-rich part of the $Bi_2O_3-V_2O_5$ diagram.[132,133] The equilibrium limit according to the formulas $2Bi_2O_3$ and xV_2O_5 was determined to be 0.96.[132]

Following the initial paper of Abraham et al.[122] on BICUVOX material, >100 publications have appeared about the synthesis, electrochemical characterization, and structural studies of BIMEVOX phases.

Because of the existence of solid solutions, the correct description needs to examine the BIMEVOX phases as part of $Bi_2O_3-V_2O_5-M_xO_y$ ternary diagrams.[132−137] Figure 21 presents an example of such a diagram for M_xO_y = ZnO. As the zinc proportion increases, the structure of the stabilized phase changes from α- to β-type and then to γ-type. The most striking feature is that there is no extension off the $Bi_4V_{2-2x}Zn_{2x}O_{11}$ line toward the (V + Zn)-rich part of the diagram. This feature was reported as being common whatever the nature of M_xO_y. There was some discrepancies about that conclusion with other authors.[135−137] Lazure et al.[134] carefully examined that point for a BICOVOX solid solution. By means of density measurements and X-ray structure determinations, these authors eliminated the possibility for any cations to be located in interstitial sites. In all the area of the solid solution, the ratio $\sum$[atoms in Bi sites ($Bi_2O_2^{2+}$ sheets)]/$\sum$(atoms in V sites) remains constant and equal to 2, which means that both Bi and Co can substitute for V sites, leading to an extension from $Bi_4V_2O_{11}$ only toward Bi_2O_3 and/or M_xO_y. Figure 22 summarizes through the periodic table, the elements that have been shown to substitute for the vanadium (and in some case for the bismuth) in $Bi_4V_2O_{11}$.

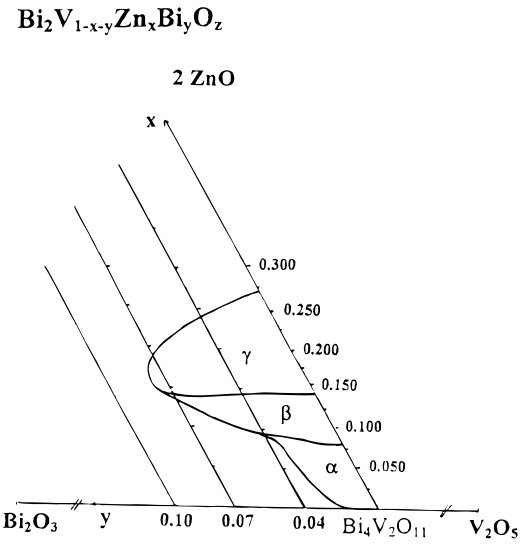

Figure 21. Domains of stability of α-, β-, and γ-polymorphs in $Bi_2O_3-V_2O_5-ZnO$ diagram. Reprinted with permission from ref 132. Copyright 1996 Elsevier.

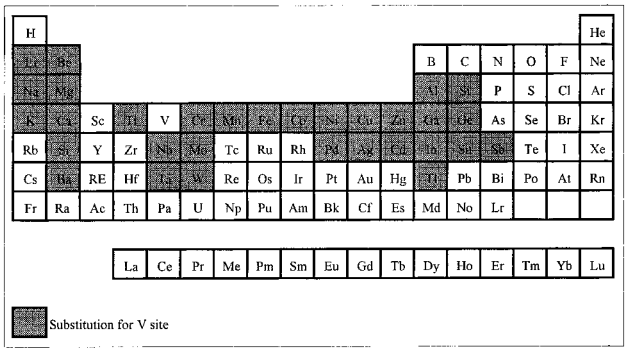

Figure 22. Table of the elements that have been shown to substitute for V in $Bi_4V_2O_{11}$.

Different single-valent substitutions for vanadium, Li^+,[138] Na^+,[136] and K^+,[137] were found to be possible at different doping levels. The Li phase belongs to the α-type structure for $x = 0.10$ and to the γ-type for $x = 0.20$. However, the occurrence of a jump in the conductivity curve of the $x = 0.20$ sample is not in agreement with the usual behavior of the γ phase. At least for this reason, the σ value remains rather low (0.25×10^{-6} S cm^{-1} at 500 K). In their study, Lee et al.[137] concluded from electron probe microanalysis, that Na-doped ($x = 0.10$) materials were single phase whereas the K-doped materials were polyphasic with very little amount of K present in the main BIMEVOX phase. Clearly, the M^+-doped materials do not offer any significant advantages.

The family of M^{2+}-substituted phases has been the most widely investigated. From an historical point of view, the Cu^{2+} derivative has been the first reported member of the BIMEVOX family. It also later appeared that the copper phase is one of the most (may be the most) attractive because of its very high conductivity: 10^{-2} S cm^{-1} at 350 °C.[139] As a consequence, many electrochemical characterizations of this phase have been performed,[123,126,127,135,140−143] all leading to the conclusion that the BICUVOX phase exhibits an exceptional oxide ion conductivity at low temperature (<500 °C). The conductivity is ~2 orders of magnitude higher than that of other oxide ion conductors in this temperature range. Many other M^{2+} substitutions have

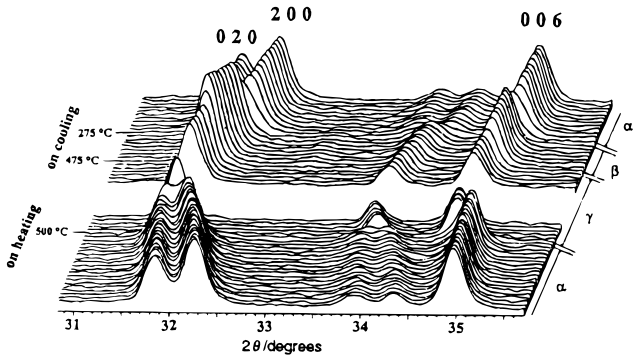

Figure 23. X-ray diffraction powder pattern for $Bi_2V_{0.95}Co_{0.05}O_\delta$ as a function of the temperature. Reprinted with permission from ref 134. Copyright 1995 Royal Society of Chemistry.

been performed with Co^{2+},[134,135,141,144] Ni^{2+},[141,145,146] Zn^{2+},[132,135,138,146] Mg^{2+},[141,147] Ca^{2+},Sr^{2+},[135,148] and Pd^{2+}.[141] Depending on the cation, they lead to stabilize the β- or the γ-type phase. For instance, along the $Bi_2V_{1-x}Zn_xO_{5.5-3x/2}$ line, the β phase is stable for $0.075 < x \leq 0.13$ and the γ phase for $0.13 < x \leq 0.25$.[132] The evolution as a function of the temperature of the α- or β-substituted phase can be rather complex and different upon heating or cooling. Figure 23 represents the XRD powder pattern of a $Bi_2V_{0.95}Co_{0.05}O_\delta$ sample.[134] On heating, there is a direct $\alpha \Rightarrow \gamma$ transition, whereas two successive $\gamma \Rightarrow \beta$ and $\beta \Rightarrow \alpha$ transitions occur on cooling. This result underlines the high sensitivity of some of these phases to the thermal history, and this parameter will have to be taken into account for application of BIMEVOX phases.

The M^{3+} cation can also substitute for $V^{5+}$and such doped phases have been obtained with Al^{3+},[138,141] Cr^{3+} and Fe^{3+},[149] In^{3+},[141] and Y^{3+} and La^{3+} [147] and, in a limited amount, with rare-earth cations (<5 mol % for Gd^{3+} and Nd^{3+}).[150] In the latter case, the substitution probably occurs on the bismuth sites. The conductivity reported for a La-substituted phase is 1.4×10^{-4} S cm^{-1} at 300 °C and 1.1×10^{-1} S cm^{-1} for an Al-doped phase at 600 °C.[147] The BICRVOX family only belongs to the α-type. When the substitution rate x in $Bi_4V_{2-x}Cr_xO_{11-x}$ is >0.05, a direct reversible $\alpha \leftrightarrow \gamma$ phase transition occurs for all compositions of the solid solution and the conductivity at low temperature dramatically decreases compared with that of α-$Bi_4V_2O_{11}$. Substitution for V^{5+} with Fe^{3+} leads successively to α-, β-, and γ'-type phases with increasing amounts of Fe. The best performance at low temperature is $\sim 10^{-4}$ S cm^{-1} at 300 °C.

In addition to Ge^{4+}, which has been mainly investigated for its ferroelectric characteristics,[138] Ti^{4+} has been the most widely characterized derivative from the Me^{4+} BIMEVOX because of its especially high ionic conductivity. For Goodenough et al.,[141,151] the most promising composition is $Bi_4V_{1.8}Ti_{0.2}O_{11-\delta}$. Yan et al.[152] analyzed the conductivity variation as a function of the Ti^{4+} content. They conclude that the highest ionic conductivity is observed in $Bi_4V_{1.70}Ti_{0.30}O_{10.85}$ ($\sigma_{500K} = 4 \times 10^{-4}$ S cm^{-1}) among the four M^{4+}-substituted phases they studied (M = Pb, Zr, Sn, Ti). The conductivity varies in the order $\sigma_{(Ti)} > \sigma_{(Sn)} > \sigma_{(Zr)} > \sigma_{(Pb)}$. This trend is in agreement with the decreasing of the total activation energy according to Kilner et al.[153] These authors pointed out the importance of the defect pairs that are formed due to the interaction between oxide ion vacancies and aliovalent cations in substituted oxides; that is, the larger the mismatch between host and dopant cation radius, the higher the association energy. Yang et al.[154,155] prepared Mn derivatives starting from MnO_2 as the dopant. They evidenced the tetragonal γ phase for 10−25% of Mn dopant on the vanadium sites. Magnetic susceptibility measurements indicated that the manganese ions are predominantly present as Mn^{3+} ions. At high temperature (T > 650 °C), some Mn^{3+} is reduced to Mn^{2+}. The transference number ranges from 0.67 at 550 °C to 0.82 at 850 °C for $Bi_2V_{0.8}Mn_{0.2}O_{5.3}$. Measurements of the oxygen permeation flux lead to values close to 1.5×10^{-8} mol s^{-1} cm^{-2} at 800 °C. These values are significantly lower than those obtained with $SrCo_{0.8}Fe_{0.2}O_{3-x}$.

Isovalent M^{5+} substitutents, such as Sb, Nb, and Ta, are known to predominantly accommodate octahedral coordination. They lead to the largest domain of solid solution.[141,156] This result is also likely due to the equality of charge between the doping cation and the vanadium, thereby keeping constant the number of oxygen vacancies. Nearly 50% of the vanadium can be substituted by Sb, Nb, or Ta. Regarding the conductivity values[156] for the same compositions, antimony phases exhibit higher performances than niobium analogues. The σ values obtained with $Bi_4V_{2-x}Sb_xO_{11}$ ($\sigma = 10^{-2}$ S cm^{-1} at 320 °C) are similar to those obtained with the best BIMEVOX previously described (Me = Cu or Ti). This similarity makes these derivatives especially attractive.

As previously pointed out, the $Bi_4V_2O_{11}$ structure is closely related to that of Bi_2WO_6 or Bi_2MoO_6. Surprisingly, Goodenough et al.[141] did not succeed in synthesizing ME = W or Mo BIMEVOX phases. According to Vannier et al.[157] and Mairesse,[158] such phases do exist. The $Bi_2V_{1-x}Mo_xO_{5.5-x/2}$ solid solution is obtained up to $x = 0.225$. For $x < 0.05$, the solid solution belongs to the α-type, whereas for $0.05 < x < 0.225$, it becomes the β-type. Because the V^{5+}/Mo^{6+} substitution implies a decrease of the number of oxygen vacancies and because the conductivities remain practically the same over all the composition range, it clearly appears that the predominant parameter determining the conductivity performances is the specific structural arrangement. The oxide ion/vacancies number ratio is only a second-order parameter.

Another interesting example of $V^{5+} \Rightarrow M^{6+}$ substitution is provided by U^{6+} cations. Bismuth uranate Bi_2UO_6 also exhibits a high oxide ion conductivity at moderate temperatures.[159] Figure 24 emphasizes some similarities between $Bi_4V_2O_{11}$ and Bi_2UO_6 structures. Both are layered structures with alternating octahedra-based (vanadium) or bipentagonal pyramidal-based (uranium) layers and Bi−O layers. However, in BIMEVOX materials, the conduction undoubtedly occurs in the perovskite (octahedra) layer whereas in Bi_2UO_6 it has been suggested that oxide ion migration would occur in Bi−O layers.[159] Thery et al.[160] have reported a $Bi_2V_{1-x}U_xO_{5.5+x/2}$ solid solution in the range $0 \leq x \leq 0.125$. For $0 \leq x \leq 0.06$, the solid solution belongs to the α-type, whereas a γ-type occurs for higher x values. This material constitutes the only example of an M^{6+}-doped γ-type phase. Figure 25 represents the Arrhenius plots of conductivity for BIUVOX.10 and BIUVOX.125 compared with that of BICUVOX.10 and Bi_2UO_6. The high-temperature conductivity is very close to that of

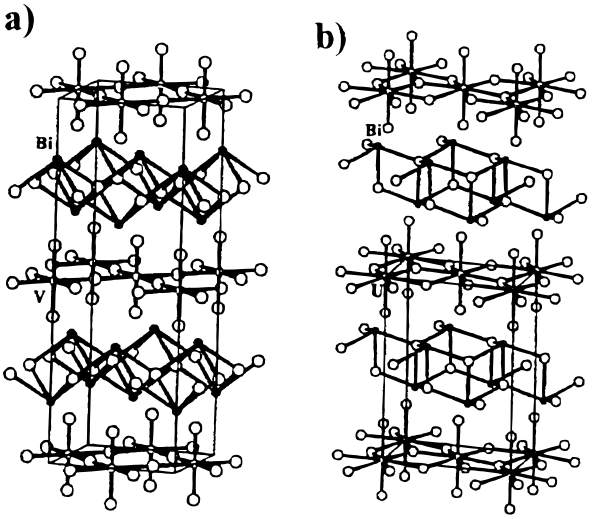

Figure 24. Comparison between (a) $Bi_4V_2O_{11}$ and (b) Bi_2UO_6 structures. Reprinted with permission from ref 160. Copyright 1996 Elsevier.

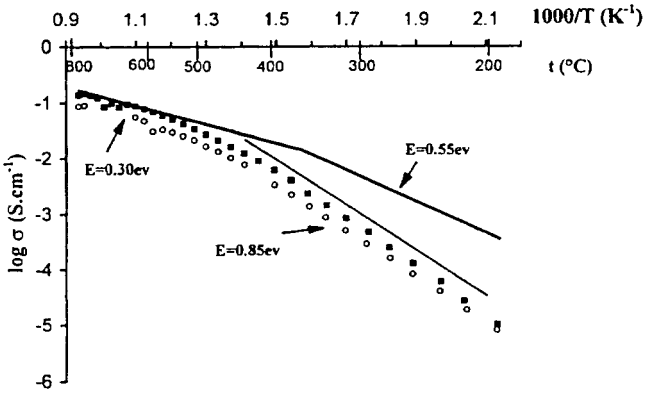

Figure 25. Comparison between (●) BIUVOX.10 and (○) BIUVOX.125 to (—) BICUVOX.10 and (−) Bi_2UO_6 conductivities.

the BICUVOX phase. However, because of the higher activation energies both in the γ (high-temperature) and γ' (low-temperature) domains, the BIUVOX conductivity becomes at 200−300 °C roughly an order of magnitude lower than that of BICUVOX.

Some double-substituted (Me = M, M′) BIMEVOX phases have also been reported.[161] Vannier et al.[161] compared the performances of such phases to that of a BICUVOX.10 phase. They introduced two kinds of atoms in vanadium site (Cu−Ni, Cu−Zn, Ni−Zn, Cu−Mo) and performed simultaneous substitution for bismuth and vanadium sites (Bi−Pb and V−Cu, Bi−Pb and V−Mo). They did not observe any improvement in the oxide ion conduction properties. However, it was emphasized that such an approach could be useful to optimize other parameters such as mechanical properties or thermodynamic activity, which can be determining for practical applications.

To use BIMEVOX as membrane materials, an important parameter is the behavior of these materials as a function of $p(O_2)$. Chadwick et al.[162,163] performed measurements of thermoelectric power (θ) on $Bi_4V_2O_{11}$ and BICUVOX samples. They observed a complex and unusual variation of θ. At moderate temperature, (<850 K), the dependence of θ versus $p(O_2)$ for all the samples is indicative of ionic conduction at high oxygen

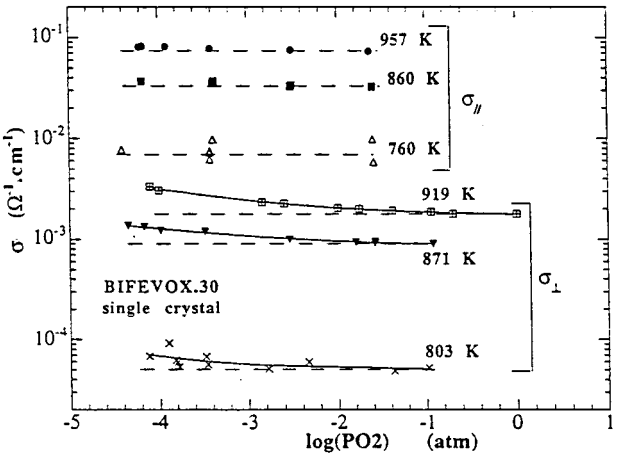

Figure 26. Conductivity variation in || and ⊥ direction to layers in BIFEVOX material as a function of $p(O_2)$.[164]

partial pressures (>100 Pa). However, at higher temperatures, the materials do not show the expected dependence with $p(O_2)$ for an ionic conductor. It is even quite unusual. A tentative explanation for the apparent contradiction between thermoelectric power and conductivity measurements is that there are changes in the oxidation states of the cationic dopants at high temperature. These changes would occur preferentially in the surface regions and therefore affect the sample/electrode interface composition and then the thermoelectric power. Iharada et al.[140] have investigated the electrical properties dependence of a BICUVOX.10 sample with $p(O_2)$. They observed a few percent increase of the n-type bulk conductivity as the $p(O_2)$ decreased. This variation was also observed to be temperature dependent; that is, the lower the temperature, the smaller the increase. Additional electrode polarization experiments revealed that, in marked contrast with stabilized zirconia, the electrode polarization decreases as the $p(O_2)$ is reduced. This result implies that the electronic conductivity has a determining influence on the electrode polarization. The nature of electronic carriers was also shown to be influenced by the nature of the dopant.[164] At temperatures higher than ∼500 °C, an n-type conductivity is observed for oxygen pressure lower than $\sim 10^{-2}$ atm for Cu-, Ni-, and Fe-substituted materials, whereas a p-type conductivity is obtained with BICOVOX for oxygen pressure $>10^{-4}$ atm. Because of the anisotropic character of the conductivity, Fouletier et al.[164] investigated the variation of the conductivity versus oxygen pressure in perpendicular directions on a single crystal. Figure 26 shows that the electronic conductivity increases more rapidly for $\sigma_\perp$ than for $\sigma_{||}$ when the oxygen partial pressure decreases.

The nature and reversibility of the modifications that may affect $Bi_4V_2O_{11}$[165] and BIMEVOX[166,167] phases under reducing conditions have also been investigated by Huve et al.[165] using high-temperature TEM, high-resolution electron microscopy, and in situ XRD. At 330 °C, under hydrogen atmosphere, α-$Bi_4V_2O_{11}$ progressively and reversibly converts into a γ-type structure. Because of the presence in the material of some V^{4+} ions revealed by electronic paramagnetic resonance, this transformation was interpreted as an in situ doping corresponding to the formation of a $Bi_2(V^{5+}_{1-x}V^{4+}_x)O_{5.5-x/2}$ solid solution, the doping cation being the vanadium itself at a lower valence state. As the reduction goes

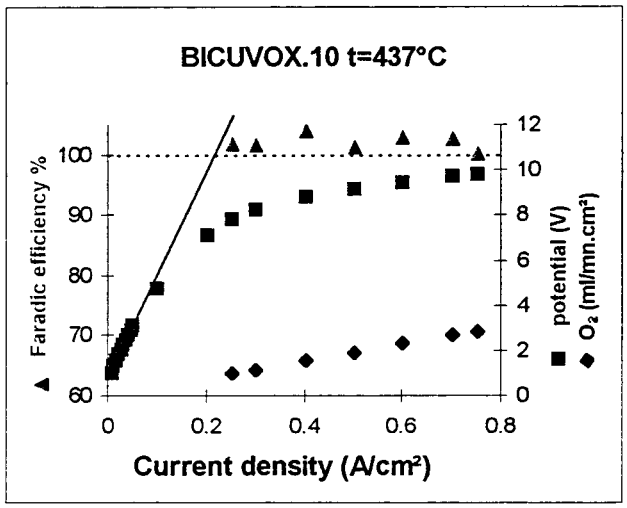

Figure 27. Variation of cell potential, O_2 production, and Faradic efficiency as a function of the current density in BICUVOX.10 at 486 °C.[168]

on, a new phase appears later, corresponding to $Bi_4V_2O_{10.66}$.[169] This ordered phase, that can be written $Bi_2(V^{5+}_{1-x}V^{4+}_x)O_{5.5-x/2}$ with $x = 0.33$, differs from the γ-type solid solution from a structural point of view. It is characterized by the transformation of the 2-dimensional vacancy conduction layer into an independent set of parallel ribbons without any vacancies. So, the new phase is an insulator. This means, that reaching this stage under operating conditions would have catastrophic consequences on the electrolyte behavior. Before that dead point, mixed conductivity occurs in the material. Similar conclusions were deduced from experiments performed on different BIMEVOX phases.

In a recent paper, Boivin et al.[168] emphasized that it was possible to take advantage of these results. They separated oxygen from air with a BIMEVOX membrane (ME = Cu, Co, Zn) constituted by a ceramic BIMEVOX pellet (diameter, 1.6 cm; thickness, 0.2 cm) co-sintered with metallic grids on opposite faces. Using a BICUVOX electrolyte, oxygen was transferred at 437 °C with 100% efficiency using high current densities (up to 800 mA cm^{-2}). This result corresponds to an oxygen flux of 2.1 μmol cm^{-2} s^{-1}. For the sake of comparison, the oxygen flux obtained with a fluorite-type $(Bi_2O_3)_{0.75}$-$(Er_2O_3)_{0.25}$ membrane at 630 °C was equal to 0.5−0.7 μmol cm^{-2} s^{-1}.[170] Figure 27 illustrates the specific behavior of such a device at 486 °C. The most striking feature is the progressive departure from the Ohm's law as the current density increases. This departure was interpreted as a progressive decrease of the effective electrolyte thickness which, as the current density increases, progressively and reversibly converts into $Bi_2(V^{5+}_{1-y-x}V^{4+}_xCu_y)O_{5.5-y-x/2}$, an efficient mixed electronic−ionic electrode material. For a fixed current density, the system quickly reaches an equilibrium state. The limiting current corresponds to the minimum electrolyte thickness required to prevent electrons from percolating through the membrane. Because of the catalytic increasing efficiency toward oxygen dissociation of the electrode material as the temperature rises, this limit also depends on the operating temperature.

Such properties are also dependent on the microstructure of the materials. The grain boundaries, the porosity, and the number and nature of defects strongly influence the electrical and mechanical properties. Different techniques for the synthesis of BIMEVOX phases have been examined. Bhattacharya et al.[171] synthesized γ-type $Bi_4V_2O_{11}$ from bismuth nitrate hydrate and ammonium vanadate. They obtained an amorphous phase that becomes fully crystalline at 593 K, with an average crystallite size of ~10 nm. Vaidhyanathan et al.[172] prepared α-$Bi_4V_2O_{11}$ using microwave irradiation starting from the stoichiometric mixture of Bi_2O_3 and V_2O_5. The starting mixture was exposed for 15 min to the microwaves and then annealed for 2 h at 973 K. The authors emphasize that the non-annealed samples during DSC runs exhibit only a very weak endothermic $\alpha \rightleftharpoons \beta$ peak. This result could indicate a limited reaction after the microwave irradiation alone. A sol−gel synthesis of α-$Bi_4V_2O_{11}$ has been proposed by Pell et al.[173] Starting from vanadium 2-methoxyethoxide prepared by azeotropic distillation of V_2O_5 in excess 2-methoxyethanol and benzene and from soluble bismuth acetate obtained from Bi_2O_3 and glacial acetic acid boiled under flowing nitrogen, they obtained α-$Bi_4V_2O_{11}$ after heating the gel at 110 °C and the resulting powder up to 725 °C. Some traces of $BiVO_4$ were detected in the final product. A $BiVO_4$-free α-$Bi_4V_2O_{11}$ powder was obtained at 450 °C using bismuth 2-methoxyethoxide made by the alcoholysis of $Bi(N(Si(CH_3)_3)_2)_3$ instead of bismuth acetate. Thin films of α-$Bi_4V_2O_{11}$ have been deposited by Viswanathan et al.[174] on an amorphous quartz and polycrystalline silicon substrates by radio frequency sputtering technique. Aiming at improving ferroelectric properties, Shanta and Varma[175] fabricated grain-oriented $Bi_4V_2O_{11}$ ceramics via a liquid-phase-aided two-stage sintering process. Addition of known amounts of KCl to pre-reacted $Bi_4V_2O_{11}$ powder led, after heating at 1025 K, washing with water, and new final sintering at 1025 K of a cold-pressed pellet, to a grain-oriented ceramic with an orientation factor of 0.79. Unlike the randomly oriented ceramic, this new ceramic exhibits a significant piezoelectric effect. In addition to new synthesis routes for the parent phase $Bi_4V_2O_{11}$, similar attempts have been made for various substituted phases. Sant et al.[176] have grown BICUVOX.10 thin films by pulsed laser deposition on polycrystalline BeO and (100) MgO substrates. Using atomic force microscopy (AFM), they evidenced a spiral growth and, for samples grown at 600 °C, a very low surface roughness. Pell et al.[177] obtained defect-free films of BICUVOX.10 on $SrTiO_3$ substrates by the pulsed laser deposition technique. Muller et al.[178] induced room-temperature orientation in BICOVOX.15 powdered samples mixed with 50% Araldite glue. The orientation was obtained by applying a 7 T magnetic field. Texture analyses revealed a [001] fiber texture with a random in-plane orientation. Combined with an uniaxial pressure, this technique leads to ceramics with physical properties close to those measured on single crystals. Recently, a new process for manufacturing inorganic mixed ionic−electronic conductive membranes for separating oxygen from oxygen-containing gaseous mixtures has been proposed by Carolan et al.[179] The membranes are formed by depositing a porous layer of BICUVOX.10 on the outer surface of a porous MgO tube using a slip made from calcined BICUVOX powder. The BICUVOX pores are then closed using metallic nickel deposited by organometallic chemical vapor deposition. Tubes manufactured with such a composite membrane were shown to

allow oxygen to be selectively transported at 700−750 °C from an outer 6 atm air pressure to the interior of the tube at approximately atmospheric pressure.

$n > 1$ Aurivillius Electrolytes. The first reported $n > 1$ Aurivillius family oxide electrolytes were made in 1997 by Kendall et al.[180,181] and Thomas et al.[182] These materials are described as intergrowths derived from Aurivillius phases and brownmillerite-related phases. As described before, a brownmillerite layer is simply an oxygen-deficient perovskite layer in which the oxygen vacancies are ordered along the [101] direction. As ordering in this new phase was shown to be strongly dependent on both the temperature and the thermal history and in the absence of any precise experimental proof from, for instance, neutron diffraction, the distinction between a brownmillerite-like layer and a partly or fully disordered oxygen-deficient perovskite layer becomes a bit philosophical. Whatever the preferred description, several new oxide electrolytes corresponding to $n = 3$ ($Bi_2Sr_2M'_2M''O_{11.5}$, with M′ = Nb, Ta and M″ = Al, Ga) and $n = 4$ ($BaBi_4Ti_3MO_{14.5}$, with M = Sc, In, Ga) have been reported. The general conductivity behavior is characterized during the first heating cycle by a jump of the conductivity occurring between 700 and 850 °C. On cooling, a semistabilized state is generally observed, with conductivity values 1 or 2 orders of magnitude higher than during the first heating run. This state is usually maintained during the first part of the next heating but, finally, the conductivity drops to the value observed during the initial run. The proposed mechanism associates the jump observed upon heating to an order−disorder transition of the oxygen vacancies in the perovskite layer as usual in brownmillerite structures (see $Ba_2In_2O_5$). The vacancy-disordered state remains stable below the initial onset temperature upon subsequent cooling. The best conductivity values ($\sigma = 4.9 \times 10^{-2}$ S cm^{-1} at 900 °C) are obtained with $BaBi_4Ti_3InO_{14.5}$. The corresponding activation energy in the high-temperature domain is equal to 0.35 eV. Similar results have been obtained by Pham et al.[183,184] for Aurivillius phases corresponding to $n = 2$. The phase $NaBi_2Nb_2O_{8.5}$ exhibits a discontinuous change in the Arrhenius plot of the conductivity at 860 °C. At 900 °C, the σ value reaches 10^{-2} S cm^{-1}. An entire solid solution $Ca_{1-x}Na_xBi_2Nb_2O_{9-x/2}$ was observed. The sample with $x = 0.1$ displays no significant change in conductivity compared with the stoichiometric phase. All samples with $x \geq 0.2$ exhibit a conductivity discontinuity in the range 850−900 °C attributed to the disordering of oxygen vacancies accompanied by a lowering of the activation energy. The conductivities of the high-temperature disordered phases increase first with x and then saturate for $x > 0.4$. If one assumes that the preexponential factor in the Arrhenius equation is proportional to the carrier concentration, this result suggests that not all the oxygen vacancies participate in the conduction process in the high-temperature phase. Saturation occurs for $x > 0.4$ (i.e., for 0.2 oxygen vacancies per formula unit). This result is in agreement with the nearly independent character of the BIMEVOX conductivity whatever the dopant cation nature.[184] The order of magnitude of conductivity values for the $n > 1$ Aurivillius phases is significantly lower than the $n = 1$ BIMEVOX phases. This result emphasizes the role of the bismuth lone pair on the oxide conduction process. In the BIMEVOX phases, the ReO_3-type layer is sandwiched between two Bi_2O_2 layers. All the lone pairs point toward this layer and can therefore dynamically assist the oxide ion migration, leading to an enhanced overall mobility.

Conclusion

Over the past decade, considerable improvements have been made in the field of fast oxide ion conductors. The synthesis of a new family of materials leading to both an increase of the performances and a better understanding of the fundamentals of oxide ion conduction mechanisms are together responsible for these improvements. New fields of applications have appeared because of the significant reduction of operating temperatures of some of these new phases. In addition to the intrinsic basic properties, the role of microstructure has been emphasized, leading to the development of new routes for solid synthesis and new techniques for ceramic manufacturing. Composite materials with optimized individual properties and good chemical and mechanical compatibility have also been the object of numerous research works. Solid-state inorganic chemists have brought a first-order contribution to these improvements. Two main approaches appear now as realistic alternatives for manufacturing dense-oxide ion membranes. In addition to the well-known zirconia-based oxides that exhibit unique specificities, a new series of solid solutions based on the $LaGaO_3$ parent compound are generating an increasing interest for the development of efficient SOFCs. Recent evidence indicates that fast ion conductors seem the most promising materials for low-temperature, current-driven membrane applications ($T < 600$ °C). From this point of view, the BIMEVOX phases presently exhibit the most attractive properties for the electrochemical separation of oxygen gas at high and intermediate partial pressure. Their ability to support high current densities without degradation is a determining advantage. At higher temperatures, mixed monophasic or polyphasic ionic−electronic conductors appear as an attractive solution with possible large-scale applications in pressure-driven membranes and syn-gas synthesis. The new mixed conductor $SrFeCo_{0.5}O_x$ fulfills many of the requirements (good chemical stability, low activation energy, equilibrated balance between ionic and electronic conductivities, high oxygen fluxes). The frontier between both types of materials is sometimes very tenuous, some pure ionic conductors can partly act as a mixed conductor under specific operating conditions leading the same material to be in charge of several functions of different nature simultaneously. This point can be of a great technological interest because it allows one to limit the number of components and eliminates, at least partly, some of the chemical and mechanical compatibility problems. However, new advances are still needed; for example, limiting material aging, particularly under high current densities, and improving existing synthesis routes and developing new routes. In this review we have tried to emphasize some of the solutions that are under examination. Whatever the material problem to address, a strong interaction between synthesis chemistry and precise structural and electrochemical characterizations will be one of the keys to win this challenge.

Acknowledgment. The authors thank Pr. Guy Nowogrocki for fruitful discussions and for helping them

to prepare this review.

References

(1) Azad, A. M.; Larose, S.; Akbar, S. A. *J. Mater. Sci.* **1994**, *29*, 4135.
(2) Kendall, K. R.; Navas, C.; Thomas, J. K.; Zur Löye, H. C. *Solid State Ionics* **1995**, *82*, 215.
(3) Kendall, K. R.; Navas, C.; Thomas, J. K.; Zur Löye, H. C. *Chem. Mater.* **1996**, *8*, 642.
(4) Shuk, P.; Wiemhöfer, H. D.; Guth, U.; Göpel, Greenblatt, M. *Solid State Ionics* **1996**, *89*, 179.
(5) Navas, C.; Zur Löye, H. C. *Solid State Ionics* **1997**, *93*, 171.
(6) Steele, B. C. H. *Curr. Opin. Solid State Mater. Sci.* **1996**, *1*, 684.
(7) Kudo, T. *The CRC Handbook of Solid State Electrochemistry*; Gelling, P. J., Bouwmeester, H. J. M., Eds.; CRC Press: Boca Raton, 1997; p 195.
(8) Inana, H.; Tagawa, H. *Solid State Ionics* **1996**, *83*, 1.
(9) Badwal, S. P. S.; Ciacchi, F. T.; Drennan, J. *11th International Conference on Solid State Ionics*, 1997, Honolulu.
(10) Yahiro, H.; Baba, Y.; Eguchi, K.; Arai, H. *J. Electrochem. Soc.* **1988**, *135*, 2077.
(11) Mehta, K.; Hong, S. J.; Fue, J. F.; Virkar, A. *Proceedings of the 3rd International Symposium on S.O.F.C.*; Singhal, S. C., Iwahara, H., Eds.; Electrochemistry Society: 1993; p 92.
(12) Sammes, N. M.; Tompsett, G.; Cai, Z. *11th International Conference on Solid State Ionics*, 1997, Honolulu.
(13) Nigara, Y.; Mizusaki, J.; Ishigame, M. *Solid State Ionics* **1995**, *79*, 208.
(14) Takahashi, T.; Iwahara, H.; Nagai, Y. *J. Electrochem. Soc.* **1970**, *117*, 244.
(15) Harwig, H. A. *Z. Anorg. Allg. Chem.* **1978**, *444*, 151.
(16) Harwig, H. A.; Weenk, J. W. *Z. Anorg. Allg. Chem.* **1978**, *444*, 111.
(17) Battle, P. D.; Catlow, C. R. A.; Drennan, J.; Murray, A. D. *J. Phys.* **1983**, *C16*, L561.
(18) Depero, L. E.; Sangaletti, L. *J. Solid State Chem.* **1996**, *122*, 439.
(19) Harwig, H. A.; Gerards, A. G. *J. Solid State Chem.* **1978**, *265*, 26.
(20) Denis-Dumelie, M.; Nowogrocki, G.; Boivin, J. C. *Br. Ceramic Proc.* **1988**, *43*, 151.
(21) Dumelie, M.; Nowogrocki, G.; Boivin, J. C. *Solid State Ionics* **1988**, *28*−*30*, 524.
(22) Boukamp, B. A.; Van Hassel B. A.; Vincke, I. C.; De Vries, K. J.; Burggraaf, A. J. *Electrochim. Acta* **1993**, *38*(14), 1817.
(23) Levin, E. M.; Roth R. S. *J. Res. Nat. Bur. Stand. Phys. Chem.* **1964**, *68A*, 197.
(24) Boivin, J. C.; Thomas, D.; Tridot, G. *C. R. Acad. Sci.* **1969**, *268C*, 1149.
(25) Takahashi, T.; Iwahara, H.; Nagai, Y. *J. Appl. Electrochem.* **1972**, *2*, 97.
(26) Boivin, J. C.; Tridot, G. *C. R. Acad. Sci.* **1974**, *278C*, 865.
(27) Conflant, P.; Boivin, J. C.; Tridot, G. *C. R. Acad. Sci.* **1974**, *279C*, 457.
(28) Conflant, P.; Boivin, J. C.; Thomas, D. *J. Solid State Chem.* **1976**, *18*, 133.
(29) Takahashi, T.; Iwahara, H. *Mater. Res. Bull.* **1978**, *13*, 1447.
(30) Guillermo, R.; Conflant, P.; Boivin, J. C.; Thomas, D. *Rev. Chim. Miner.* **1978**, *15*, 153.
(31) Takahashi, T.; Iwahara, H.; Arao, T. *J. Appl. Electrochem.* **1975**, *5*, 197.
(32) Takahashi, T.; Esaka, T.; Iwahara, H. *J. Appl. Electrochem.* **1977**, *7*, 299.
(33) Verkerk, M. J.; Burggraaf, A. J. *J. Appl. Electrochem.* **1980**, *10*, 677.
(34) Watanabe, A.; Kikuchi, T. *Solid State Ionics* **1986**, *21*, 287.
(35) Dodor, P. J.; Tanaka, J.; Watanabe, A. *Solid State Ionics* **1987**, *25*, 177.
(36) Joshi, A. V.; Kulkarni, S.; Nachlas, J.; Diamond, J.; Weber, J. *J. Mater. Sci.* **1990**, *25*, 1237.
(37) Kruidhof, K.; De Vries, K. J.; Burggraaf, A. J. *Solid State Ionics* **1990**, *37*, 213.
(38) Fung, K. Z.; Virkar, A. V. *J. Am. Ceram. Soc.* **1991**, *74*, 1970.
(39) Baek, H. D.; Virkar, A. V. *J. Electrochem. Soc.* **1992**, *138*, 3174.
(40) Vlasov, A. N.; Butorina, O. O. *Russ. J. Electrochem.* **1993**, *29*, 1290.
(41) Iwahara, H.; Esaka, T.; Sato, T. *J. Solid State Chem.* **1981**, *39*, 173.
(42) Verkerk, M. J.; Burggraaf, A. J. *J. Electrochem. Soc.* **1981**, *128*, 75.
(43) Esaka, T.; Iwahara, H.; Kunieda, H. *J. Appl. Electrochem.* **1982**, *12*, 235.
(44) Esaka, T.; Iwahara, H. *J. Appl. Electrochem.* **1985**, *15*, 447.
(45) Conflant, P.; Follet-Houttemane, C.; Drache, M. *J. Mater. Chem.* **1991**, *1*(4), 649.
(46) Su, P.; Virkar, A. V. *J. Electrochem. Soc.* **1992**, *139*, 1671.
(47) Kikuchi, T.; Kitami, Y.; Yokoyama, M.; Sakai, H. *J. Mater. Sci.* **1989**, *24*, 4275.
(48) Takahashi, T.; Iwahara, H.; Esaka, T. *J. Electrochem. Soc.* **1977**, *124*, 1563.
(49) Takahashi, T.; Iwahara, H. *J. Appl. Electrochem. Soc.* **1973**, *3*, 65.
(50) Watanabe, A.; Kikuchi, T. *Solid State Ionics* **1986**, *21*, 187.
(51) Watanabe, A. *Solid State Ionics* **1989**, *34*, 35.
(52) Watanabe, A. *Solid State Ionics* **1990**, *40*−*41*, 889.
(53) Watanabe, A.; Drache, M.; Wignacourt, J. P.; Conflant, P.; Boivin, J. C. *Solid State Ionics* **1993**, *67*, 25.
(54) Wachman, E. D.; Jiang, N.; Mason, D. M.; Stevenson, D. A. *Proc. Electrochem. Soc.* **1989**, *89-11*, 15.
(55) Wachman, E. D.; Ball, G. R.; Mason, D. M.; Stevenson, D. A. *Solid State Ionics* **1992**, *52*, 213.
(56) Jiang, N.; Buchanan, R. M.; Henn, F. E. G.; Marshall, A. F.; Stevenson, D. A.; Wachman, E. D. *Mater. Res. Bull.* **1994**, *29-3*, 247.
(57) Fung, K. Z.; Virkar, A. V. *Solid State Ionics* **1992**, *52*, 199.
(58) Fung, K. Z.; Chen, J.; Virkar, A. V. *J. Am. Ceram. Soc.* **1993**, *76-10*, 2403.
(59) Jiang, N.; Buchanan, R. M.; Stevenson, D. A.; Nix, W. D.; Li, J.-Z.; Yang, J.-L. *Mater. Lett.* **1995**, *22*, 215.
(60) Watanabe, A. *Solid State Ionics* **1996**, *86/88*, 1427.
(61) Drache, M.; Conflant, P.; Obbade, S.; Wignacourt, J. P. *J. Solid State Chem.* **1997**, *129*, 98.
(62) Meng. G.; Chen, C.; Han, X.; Yang, P.; Peng, D. *Solid State Ionics* **1988**, *28*−*30*, 533.
(63) Drache, M.; Conflant, P.; Boivin, J. C. *Solid State Ionics* **1992**, *57*, 245.
(64) Hu K.; Chen C.; Peng, D.; Meng, G. *Solid State Ionics* **1988**, *28*−*30*, 566.
(65) Omari, M.; Drache, M.; Conflant, P.; Boivin, J. C. *Solid State Ionics* **1990**, *40*−*41*, 929.
(66) Portefaix, N.; Conflant, P.; Boivin, J. C.; Wignacourt, J. P.; Drache, M. *J. Solid State Chem.* **1997**, *134*, 219.
(67) Huang, K.; Feng, M.; Goudenough, J. B. *Solid State Ionics* **1996**, *89*, 17.
(68) Sooryanarayana, K.; Samashekar, R.; Guru Row, T. N. *Solid State Ionics* **1997**, *104*, 319.
(69) Sillen, L. G.; Aurivillius, B. *Z. Kristallogr.* **1939**, *101*, 483.
(70) Demonchy, P.; Conflant, P.; Boivin, J. C.; Thomas, D. *C. R. Acad. Sci.* **1979**, *C289*, 317.
(71) Mercurio, D.; El Farissi, M.; Frit, B.; Reau, J. M.; Senegas, J. *Solid State Ionics* **1990**, *39*, 297.
(72) Conflant, P.; Boivin, J. C.; Nowogrocki, G.; Thomas, D. *Solid State Ionics* **1983**, *9*, 925.
(73) Boivin, J. C.; Thomas, D. *Solid State Ionics* **1981**, *3*−*4*, 457.
(74) Boivin, J. C.; Thomas, D. *Solid State Ionics* **1981**, *5*, 523.
(75) Mercurio, D.; Champarnaud-Mesjard, J. C.; Frit, B.; Conflant, P.; Boivin, J. C.; Vogt, T. *J. Solid State Chem.* **1994**, *112*, 1.
(76) Blower, S. K.; Greaves, C. *Mater. Res. Bull.* **1988**, *23*, 765.
(77) Mercurio, D.; El Farissi, M.; Champarnaud-Mesjard, J. C.; Frit, B.; Conflant, P.; Roult G. *J. Solid State Chem.* **1989**, *80*, 133.
(78) Baek, H. D.; Virkar A. V. *J. Electrochem. Soc.* **1992**, *139*, 3174.
(79) Virkat A. V. *J. Electrochem. Soc.* **1991**, *138*, 1481.
(80) Scarfe, D. P.; Bhavaraju, S.; Jacobson, A. *J. Chem. Commun.* **1997**, 313.
(81) Scarfe, D. P.; Jacobson, A. *Chem. Mater.* **1997**, *9*, 3107.
(82) Takahashi, T.; Iwahara, H. *Energy Convers.* **1971**, *11*, 105.
(83) Cook, R. L.; Sammells, A. F. *Solid State Ionics* **1991**, *45*, 311.
(84) Goodenough, J. B.; Manthiram, A.; Paramthaman, P.; Zhen, Y. S. *Solid State Ionics* **1992**, *52*, 105.
(85) Feng, M.; Goodenough, J. B. *Eur. J. Solid State Inorg. Chem.* **1994**, *31*, 663.
(86) Ishihara, T.; Matsuda, H.; Takita, Y. *J. Am. Chem. Soc.* **1994**, *116*, 3801.
(87) Ishihara, T.; Matsuda, H.; Takita, Y. *Solid State Ionics* **1995**, *79*, 147.
(88) Teraoka, Y.; Nobunaga, T.; Yamazoe, N. *Chem. Lett.* **1988**, 503.
(89) Tai, L. W.; Nasrallah, M. M.; Anderson, H. U.; Sparlin, D. M.; Sehlin, S. R. *Solid State Ionics* **1995**, *76*, 259.
(90) Tai, L. W.; Nasrallah, M. M.; Anderson, H. U.; Sparlin, D. M.; Sehlin, S. R. *Solid State Ionics* **1995**, *76*, 273.
(91) Balachandran, U.; Dusek, J. T.; Sweeney, S. M.; Poeppel, R. B.; Mieville, R. L.; Maiya, P. S.; Kleefisch, M. S.; Pei, S.; Kobylinski, T. P.; Udovich, C. A.; Bose, A. C. *Am. Ceram. Soc. Bull.* **1995**, *74*, 71.
(92) Ma, B.; Balachandran, U.; Park, J. H. *J. Electrochem. Soc.* **1996**, *143*, 1736.
(93) Goodenough, J. B.; Ruiz-Diaz, J. E.; Zhen, Y. S. *Solid State Ionics* **1990**, *44*, 21.
(94) Adler, S. B.; Russek, S.; Reimer, J.; Fendorf, M.; Stacy, A.; Huang, Q.; Santoro, A.; Lynn, J.; Baltisberger, J.; Werner, U. *Solid State Ionics* **1994**, *68*, 193.
(95) Goodenough, J. B. *Solid State Ionics* **1997**, 94, 17.
(96) Goodenough, J. B.; Manthiram, A.; Paranthaman P.; Zhen, Y. S. *Solid State Ionics* **1992**, *52*, 105.
(97) Abraham, F.; Boivin, J. C.; Mairesse, G.; Nowogrocki, G. *Solid State Ionics* **1990**, *40*−*41*, 934.

(98) Manthiram, A.; Kuo, J. F.; Goodenough, J. B. *Solid State Ionics* **1993**, *62*, 225.
(99) Turrillas, X.; Sellars, A. P.; Steele, B. C. H. *Solid State Ionics* **1988**, *28−30*, 465.
(100) Kramer, S. A.; Tuller, H. L. *Solid State Ionics* **1995**, *28−30*, 465.
(101) Tuller, H. L. *Solid State Ionics* **1997**, *94*, 63.
(102) Porat, O.; Heremans, C.; Tuller, H. L. *J. Am. Ceram. Soc.*, in press.
(103) Honnart, F.; Boivin, J. C.; Thomas, D.; De Vries, K. J. *Solid State Ionics* **1983**, *9−10*, 921.
(104) Graia, T.; Conflant, P.; Boivin, J. C.; Thomas, D. *Solid State Ionics* **1986**, *18−19*, 751.
(105) Sammes, N. M.; Philips, R. J.; Fee, M. G. *Solid State Ionics* **1994**, *69*, 121.
(106) Fee, M. G.; Long, N. J. *Solid State Ionics* **1996**, *86−88*, 733.
(107) Abraham, F.; Debreuille-Gresse, M. F.; Mairesse, G.; Nowogrocki, G. *Solid State Ionics* **1988**, *28−30*, 529.
(108) Bush, A. A.; Koshelayeva V. G.; Venevtsev, Yu. N. Proceedings of the 6th International Meeting on Ferroelectricity Kobe, 1985; *Jpn. J. Appl. Phys.* **1985**, *24*, 625.
(109) Bush, A. A.; Venevtsev, Yu. N. *Russ. J. Inorg. Chem.* **1986**, *31-5*, 769.
(110) Blinovskov, Ya. N.; Fotiev, A. A. *Russ. J. Inorg. Chem.* **1987**, *32-1*, 145.
(111) Koshelayeva V. G.; Bush, A. A.; Titov, V.; Venevtsev, Yu. N. *Russ. J. Inorg. Chem.* **1988**, *33-12*, 1815.
(112) Borisov, V. N.; Poplavko, Yu. M.; Avakyan, P. B.; Osipyan, V. G. *Sov. Phys. Solid State* **1988**, *30-5*, 904.
(113) Prasad, K. V. R.; Varma, K. B. R. *J. Phys. D: Appl. Phys.* **1991**, *24*, 1858.
(114) Varma, K. B. R. *Mater. Chem. Phys.* **1994**, *38*, 406.
(115) Prasad, K. V. R.; Varma, K. B. R. *J. Mater. Sci. Lett.* **1994**, *13*, 215.
(116) Raju Varma, K. B. R. *J. Mater. Sci.* **1994**, *29*, 2691.
(117) Varma, K. B. R. *Shankar Subbanna Mater. Res. Bull.* **1995**, *31-5*, 475.
(118) Varma, K. B. R.; Prasad, K. V. R. *Mater. Res.* **1996**, *11-9*, 2288.
(119) Shantha, K.; Varma, K. B. R. *J. Mater. Chem.* **1997**, *7−8*, 1565.
(120) Ramasesha, S. K.; Singh, A. K.; Varma, K. B. R. *Mater. Chem. Phys.* **1997**, *48*, 136.
(121) Shantha, K.; Varma, K. B. R. *Solid State Ionics* **1997**, *99*, 225.
(122) Abraham, F.; Boivin, J. C.; Mairesse, G.; Nowogrocki, G. *Solid State Ionics* **1990**, *40−41*, 934.
(123) Reiselhuber, K.; Dorner G.; Breiter, M. W. *Electrochim. Acta* **1993**, *38-7*, 969.
(124) Dygas, J. R.; Krok, F.; Bogusz, W.; Kurek, P.; Reiselhuber, K.; Breiter, M. W. *Solid State Ionics* **1994**, *70−71*, 239.
(125) Kurek, P.; Dygas, J. R.; Breiter, M. W. *J. Electroch. Chem.* **1994**, *378*, 77.
(126) Dygas, J. R.; Kurek, P.; Breiter, M. W. *Solid State Phenom.* **1994**, *39−40*, 61.
(127) Kurek, P.; Dygas, J. R.; Breiter, M. W. *Solid State Phenom.* **1994**, *39−40*, 247.
(128) Dygas, J. R.; Kurek, P.; Breiter, M. W. *Electrochim. Acta* **1995**, *40-10*, 1545.
(129) Vannier, R. N.; Mairesse, G.; Abraham, F.; Nowogrocki, G.; Pernot, E.; Anne, M.; Bacmann, M.; Strobel P.; Fouletier, J. *Solid State Ionics* **1995**, *78*, 183.
(130) Pernot, E.; Anne, M.; Bacmann, Strobel, P.; Fouletier, J.; Vannier, R. N.; Mairesse, G.; Abraham, F.; Nowogrocki, G. *Solid State Ionics* **1994**, *70−71*, 259.
(131) Sei-Ki Kim; Masaru Miyayama. *Solid State Ionics* **1997**, *104*, 295.
(132) Vannier, R. N.; Lazure, S.; Vernochet, C.; Nowogrocki, G.; Mairesse, G. *Solid State Ionics* **1996**, *90*, 117.
(133) Lee, C. K.; Sinclair, D. C.; West, A. R. *Solid State Ionics* **1993**, *62*, 193.
(134) Lazure, S.; Vannier, R. N.; Nowogrocki, G.; Mairesse, G.; Muller, C.; Anne, M.; Strobel, P. *J. Mater. Chem.* **1995**, *5−9*, 1395.
(135) Lee, C. K.; Tan, M. P.; West, A. R. *J. Mater. Chem.* **1994**, *4−9*, 1441.
(136) Watson, C. J.; Coats, A.; Sinclair, D. C. *J. Mater. Chem.* **1997**, *7−10*, 2091.
(137) Lee, C. K.; Coats, A.; West, A. R. *Powder Diffraction* **1997**, *12-4*, 245.
(138) Sharma, V.; Shukla, A. K.; Kopalakrishnan, J. *Solid State Ionics* **1992**, *58*, 359.
(139) Boivin, J. C.; Vannier, R. N.; Mairesse, G.; Abraham, F.; Nowogrocki, G. *ISSI Lett.* **1992**, *3−4*, 3.
(140) Iharada, I.; Hammouche, A.; Fouletier, J.; Kleitz, M.; Boivin, J. C.; Mairesse, G. *Solid State Ionics* **1991**, *48-3-4*, 257.
(141) Goodenough, J. B.; Manthiram, A.; Paranthaman, P.; Zhen, Y. S. *Mater. Sci. Eng.* **1992**, *B12*, 357.
(142) Krok, F.; Bogusz, W.; Jakubowski, W.; Dygas, J. R.; Bangobango, D. *Solid State Ionics* **1994**, *70−71*, 211.
(143) Fafilek, G. *11th International Conference on Solid State Ionics*, 1997, Honolulu.
(144) Essalim, R.; Tanouti, B.; Bonnet, J. M.; Reau, J. M. *Mater. Lett.* **1992**, *13*, 382.
(145) Anne, M.; Bacmann, M.; Pernot, E.; Abraham, F.; Mairesse, G.; Strobel, P. *Physica B* **1992**, *180−181*, 621.
(146) Kurek, P.; Breiter, M. W. *Solid State Ionics* **1996**, *86−88*, 131.
(147) Lee, C. K.; West, A. R. *Solid State Ionics* **1996**, *86−88*, 235.
(148) Cherrak, A.; Hubaut, R.; Barbaux, Y.; Mairesse, G. *Catal. Lett.* **1992**, *15*, 377.
(149) Joubert, O.; Ganne, M.; Vannier, R. N.; Mairesse, G. *Solid State Ionics* **1996**, *83*, 199.
(150) Prasad, K. V. R.; Subbanna, G. N.; Varma, K. B. R. *Ferroelectrics* **1995**, *166*, 223.
(151) Goodenough, J. B.; Manthiram, A.; Paranthaman, P.; Zhen, Y. S. *Solid State Ionics* **1992**, *52*, 105.
(152) Yan, J.; Greenblatt, M. *Solid State Ionics* **1995**, *81*, 225.
(153) Kilner, J. A.; Steele, B. C. H. *Nonstoichiometric oxydes*; Sorensen, O. T., Ed.; Academic Press: New York, 1981; p 233.
(154) Yang, Y. L.; Qiu, L.; Harrison, W. T. A.; Christoffer, R.; Jacobson, A. J. *J. Mater. Chem.* **1997**, *7*(2), 243.
(155) Yang, Y. L.; Qiu, L.; Jacobson, A. J. *J. Mater. Chem.* **1997**, *7*(6), 937.
(156) Joubert, O.; Jouanneaux, A.; Ganne, M.; Vannier, R. N.; Mairesse, G. *Solid State Ionics* **1994**, *73*, 309.
(157) Vannier, R. N.; Mairesse, G.; Abraham, F.; Nowogrocki, G. *J. Solid State Chem.* **1993**, *103*, 441.
(158) Mairesse, G. In *Fast Ion Transport in Solids*; Scrosati, B., et al., Eds.; Kluwer Academic: Norwell, MA, 1993; p 271.
(159) Bonanos, N. *Mater. Res. Bull.* **1989**, *24*, 1531.
(160) Thery, O.; Vannier, R. N.; R. N.; Dion, C.; Abraham, F. *Solid State Ionics* **1996**, *90*, 105.
(161) Vannier, R. N.; Mairesse, G.; Abraham, F.; Nowogrocki, G. *Solid State Ionics* **1994**, *70−71*, 248.
(162) Chadwick, A. V.; Francklin, A. J. *Philos. Mag. A* **1993**, *68-4*, 787.
(163) Francklin, A. J.; Chadwick, A. V.; Couves, J. W. *Solid State Ionics* **1994**, *70−71*, 215.
(164) Fouletier, J.; Muller, C.; Pernot, E. *Electroceramics V*; Baptista, J. L., Labrincha, J. A., Vilarinho, P. M., Eds.; University of Aveiro: Aveiro, Portugal, 1996; p 37.
(165) Huvé, M.; Vannier, R. N.; Nowogrocki, G.; Mairesse, G.; Van Tendeloo, G. *J. Mater. Chem.* **1996**, *6−8*, 1339.
(166) Lazure, S. Thesis, 1996, Lille, France.
(167) Vernochet, C. Thesis, 1997, Lille, France.
(168) Boivin, J. C.; Nowogrocki, G.; Mairesse, G.; Labrune, P.; Lagrange, G. *11th International Conference on Solid State Ionics*, 1997, Honolulu.
(169) Joubert, O.; Jouanneaux, A.; Ganne, M.; Tournoux, M. *Mater. Res. Bull.* **1992**, *27*, 1235.
(170) Mazanec, T. J.; Cable, T. L.; Frye, J. G. *Solid State Ionics* **1992**, *53−56*, 111.
(171) Bhattacharya, A. K.; Mallick, K. K.; Thomas, P. A. *Solid State Commun.* **1994**, *91-5*, 357.
(172) Vaidhyanathan, B.; Munia Ganguli, Rao, K. J. *Mater. Res. Bull.* **1995**, *30-9*, 1173.
(173) Pell, J. W.; Ying, J. Y.; Zur Löye, H. C. *Mater. Lett.* **1995**, *25*, 157.
(174) Viswanathan, M.; Thutupalli, G. K. M.; Varma, K. B. R. *Solid State Commun.* **1996**, *98*, 535.
(175) Shantha, K.; Varma, K. B. R. *Mater. Res. Bull.* **1997**, *32-11*, 1581.
(176) Sant, P.; Contour, J. P. *J. Cryst. Growth* **1995**, *153*, 63.
(177) Pell, J. W.; Auyeng, R. C. Y.; Chrisey, D. B.; Zur Löye, H. C. *Thin Solid Films* **1997**, *300*, 154.
(178) Muller, C.; Chateigner, D.; Anne, M.; Bacmann, M.; Fouletier, J.; De Rango, P. *J. Phys. D: Appl. Phys.* **1996**, *29*, 3106.
(179) Carolan, M. F.; Dyer, P. N.; Fine, S. M.; Makitka, A.; Richards, R. E.; Shaffer, L. E. U.S. Patent 5 683 797, 1997.
(180) Kendall, K. R.; Thomas J. K.; Zur Löye, H. C. *Solid State Ionics* **1994**, *70−71*, 221.
(181) Kendall, K. R.; Thomas, J. K.; Zur Löye, H. C. *Chem. Mater.* **1995**, *7*, 50.
(182) Thomas, J. K.; Kendall, K. R.; Zur Löye, H. C. *Solid State Ionics* **1994**, *70−71*, 225.
(183) Pham, A. Q.; Puri, M.; Di Carlo, J. C.; Jacobson, A. J. *Solid State Ionics* **1994**, *72*, 309.
(184) Pham, A. Q.; Yazdi, I.; Jacobson, A. J. *J. Electrochem. Soc.* **1995**, *142-5*, 1559.
(185) Heider, U.; Shank, J.; Jörissen, L.; Huggins, R. A.; Witschel, W. *Ionics* **1995**, *1*, 188.
(186) Huang, K. Q.; Feng, M.; Goodenough, J. B. *J. Am. Ceram. Soc.* **1998**, *81*, 357.
(187) Zhang, G. B.; Smyth, D. M. *Proceedings of the 2nd International Symposium on Ionic and Mixed Conducting Oxide Ceramics*; Ramanarayanan, T. A., Worrel, W. L., Tuller, H. L., Eds.; The Electrochemical Society: Pennington, NJ, 1997; p 608.

CM980236Q